UNIVERSITY OF GRONINGEN

MASTER OF SCIENCE ASTRONOMY

KAPTEYN INSTITUTE

X-shooter Observations of Carbon Enhanced Metal-Poor Stars in Sculptor

Author:
Danny SARDJAN

Supervisors:
prof. dr. Eline TOLSTOY
dr. Ása SKÚLADÓTTIR

April 28, 2020

Abstract

The true fraction of Carbon Enhanced Metal-Poor (CEMP) stars in dwarf spheroidal galaxies is poorly known. It is currently thought that there are unusually few, especially in the case of CEMP-no stars, compared to the halo of the Milky Way. CEMP-no stars are believed to have been enriched by the first zero-metallicity massive stars because they are so common among the most metal-poor stars. The more common CEMP-s stars differ from CEMP-no stars in an enhancement in Ba. It is possible that the lack of CEMP stars in dwarf spheroidal galaxies is because past spectroscopic studies of individual stars in these galaxies have tended to ignore C-rich stars as they are hard to analyse, especially with limited wavelength range spectra, due to the presence of broad, strong Carbon features over the entire spectrum. This project uses the long wavelength range of X-shooter to study three stars that have been previously identified as C-rich in the Sculptor dwarf spheroidal. We use the MARCS stellar atmosphere models in combination with TURBOSPEC to generate synthetic spectra. We compare these synthetic spectra to the observations to determine the abundance of chemical elements that have identified absorption lines in the spectrum. For the first time we have successfully measured the abundances of C, N, Fe, Y, Ba, La, Nd and determined an upper limit of Eu in these stars. All of our stars show an enhancement in C. Two of our stars also show an enhancement in s-process elements. The third star shows only a moderate enhancement in [Ba/Fe]. All of our stars are unlikely to be enhanced in r-process elements. Therefore we conclude that we have found two CEMP-s stars and one CEMP star with moderate s-process enhancement.

Contents

1 Introduction

1.1 Stellar Archaeology

Before any stars were formed the early Universe consisted of hydrogen, helium and a tiny amount of lithium. From the primordial gas the first stars were formed, the so-called Population III stars. Like present day stars, the first stars spent most of their lifetime on the main sequence converting hydrogen into helium. In later stages of stellar evolution numerous heavier elements (also called metals) are formed in the core of the star, and when stars release a stellar wind or a supernova explosion even more metals (especially heavy metals) are formed and released. Enriching the surrounding interstellar medium (ISM). New stars then form from an ISM enriched in metals which play an important role in cooling gas clouds and the nuclear fusion process within the core of the star. Over time the fraction of metals in the ISM increases as more stars evolve and further enrich the ISM.

Low mass stars have lifetimes comparable to the age of the Universe and can therefore be observed today even though they formed while the Universe was still young and the ISM only contained a fraction of the metals we find in the ISM today. In principle the photospheres of low-mass stars do not change significantly over the lifetime of the star on the main sequence. Therefore the abundance patterns of these stars typically match that of the ISM when the star was formed. To investigate the chemical abundances of these stars they need to be observed spectroscopically. Since this method is based on studying ancient remnants, this is called *stellar archaeology.*

1.2 Carbon Enhanced Metal-Poor Stars

The stars we study in this project are Carbon Enhanced Metal-Poor (CEMP) stars. These stars are defined as having [C/Fe] > 1.0 (Beers & Christlieb, 2005). Most of these known CEMP stars have been found and studied in the Milky Way halo. A survey done by Lee et al. (2013) found that the frequency of CEMP stars in the Milky Way increases for lower metallicities, with $\sim 40\%$ of stars classified as CEMP stars in the metallicity range $-3.7 < $ [Fe/H] $ < -2.4$ and up to $\sim 75\%$ for [Fe/H] < -4. The commonly accepted assumption that carbon enhancement is believed to show the imprint of yields from the early stars comes from this observational discovery. Thus these extremely low-metallicity C-rich stars provide a window into the early Universe. Understanding the origin of the abundance pattern of these stars reveals information about the chemical enrichment process in the Universe at the time these stars were formed.

CEMP stars have been divided into subclasses defined by Beers & Christlieb (2005) as follows:

CEMP	[C/Fe] > 1.0
CEMP-r	[C/Fe] > 1.0 and [Eu/Fe] > 1.0
CEMP-s	[C/Fe] > 1.0 and [Ba/Fe] > 1.0 and [Ba/Eu] > 0.5
CEMP-r/s	[C/Fe] > 1.0 and 0.0 < [Eu/Fe] < 0.5
CEMP-no	[C/Fe] > 1.0 and [Ba/Fe] < 0.0

These definitions are not set in stone and other authors employ slightly different definitions. For example Aoki et al. (2007) define a CEMP star as having [C/Fe] > 0.7. Different subclasses indicate an enhancement in particular elements. CEMP-r and CEMP-s indicate enhancements in r- (such as Eu) and s-process (such as Ba) elements respectively, while CEMP-no stars show none of these enhancements. CEMP-no stars are typically dominant at lower [Fe/H], while CEMP-s stars are more common at higher [Fe/H]. CEMP-r stars are quite rare. In Figure 1 we see the the distribution of the different subclasses as a function of metallicity in the Milky Way halo, where we can see the distinct groups.
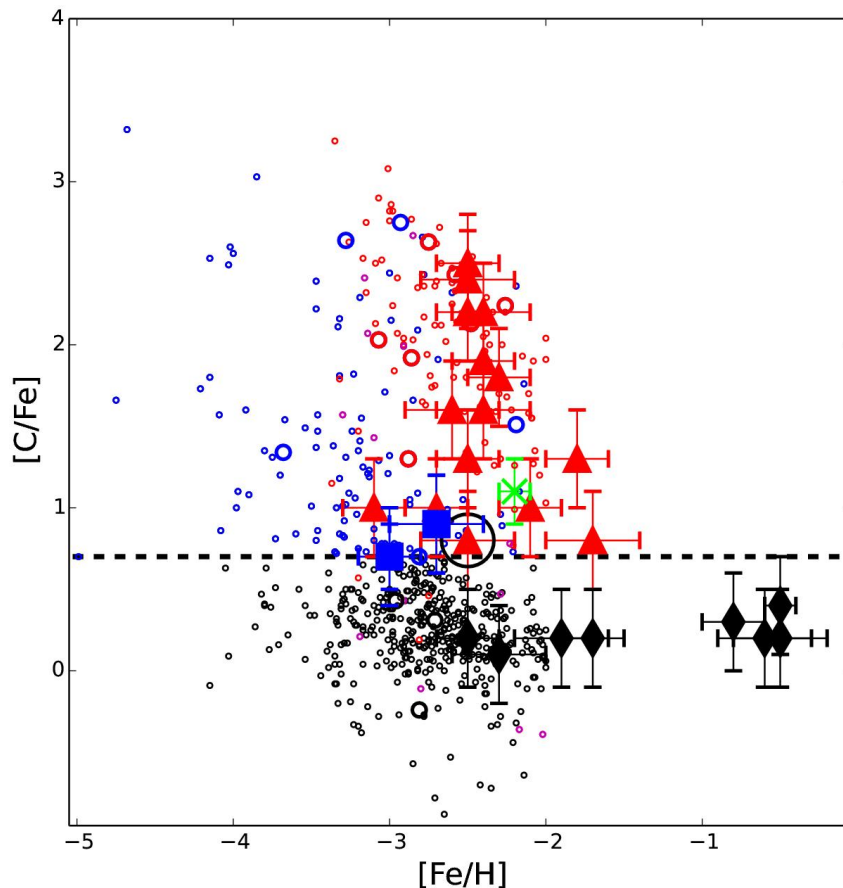

Figure 1: [C/Fe] as a function of [Fe/H] for stars in the Milky Way halo. CEMP-s stars are shown in red, CEMP-no stars in blue and carbon-normal stars are black. The green cross indicates a nitrogen enhanced metal-poor star. Figure taken from Hansen et al. (2016).

The origin of carbon enhancement is thought the be very different for CEMP-no stars compared to CEMP-s and CEMP-r stars. The origin of carbon enhancement for CEMP-s stars is well established to come from the accretion of the outer envelope of an asymptotic giant branch (AGB) star in a binary system. Stars which have undergone the AGB phase of their evolution have been able to produce s-process elements in various atmospheric layers. During this phase the star also dredges up elements from its inner regions to its atmosphere. Most of the CEMP-s stars are found to be in an easily identifiable binary

system (Starkenburg et al., 2014).

AGB stars do not host the r-process so the origin of CEMP-r stars lies elsewhere. Stellar winds are unable to provide a neutron density sufficient for the r-process to take place. Extreme events such as type II supernovae and neutron stars mergers are needed for the r-process to be possible. Therefore it is thought that the enhancement in r-process elements in stars comes from the original ISM in which the star is formed, and thus an earlier enrichment event (Sneden et al., 2008).

In the case of CEMP-no stars it is believed that their abundance pattern is the original chemical composition at birth since there is no pollution of heavier elements. This is strengthened by the fact that the binary fraction of CEMP-no stars is much lower than CEMP-s stars (Starkenburg et al., 2014). In general the carbon enhancement increases when metallicity decreases. The exact formation scenario of these stars is still unknown. One of the hypotheses is that the very first stars rotate rapidly (so-called spinstars) and could enrich the ISM with light elements such as carbon and nitrogen via stellar winds. Then this enriched ISM would form stars with an enhancement in light elements such as carbon and nitrogen while still being very low in metallicity (Maeder & Meynet, 2015). Another possibility is that the first stars undergo a supernova differently than those we observe today. An example is so-called "faint" supernovae which could retain most heavy elements in the remaining compact object because of its strong gravity and the weakness of the supernova. The ISM would become enriched with a lot of light elements (such as C, N and O) but once again very few heavier metals (such as Fe). When the next generation of stars is born, the composition of the star is the same as the ISM in which it is formed. Therefore these stars will become CEMP-no stars (Ishigaki et al., 2014). Recently another method of forming CEMP-no stars has been proposed by Hartwig & Yoshida (2019) in which inhomogeneous mixing causes some clouds to contain more carbon. It is argued that an enhancement in carbon (and oxygen) causes these clouds to collapse more quickly since these elements can cool a gas more quickly than a cloud with a lower abundance in carbon (and oxygen). Feedback of newly forming CEMP stars could quench star formation of those clouds lacking in carbon and oxygen, creating a bias in early star formation towards CEMP stars.

1.3 Challenges of CEMP Stars

The major challenge of analysing CEMP stars is the fact that carbon (and to a lesser extent, nitrogen) forms molecules which absorb photons over a wide range of wavelengths (compared to sharp absorption lines from atoms). CEMP stars are so challenging to analyse that they are often left out in larger stellar surveys even when higher resolution observations are available, such as in Hill et al. (2019).

1.3.1 Photometry

The enhanced carbon is also an issue visible in photometry. Significant flux from the star can be blocked over broad wavelength ranges (thus in certain filters) by wide carbon bands depressing the light in certain regions. To combat this we compare the photometric

temperature measurements for our sample of stars from multiple filter combinations.

1.3.2 Normalising Spectra

The molecular bands are especially difficult to deal with when trying to normalize the spectrum and accurately measure abundances. The correct determination of the continuum level of a spectrum has a major impact on the accuracy of abundance measurements. An overestimated continuum leads to measuring deeper lines (larger equivalent widths) and so higher abundances and vice versa for an underestimated continuum.
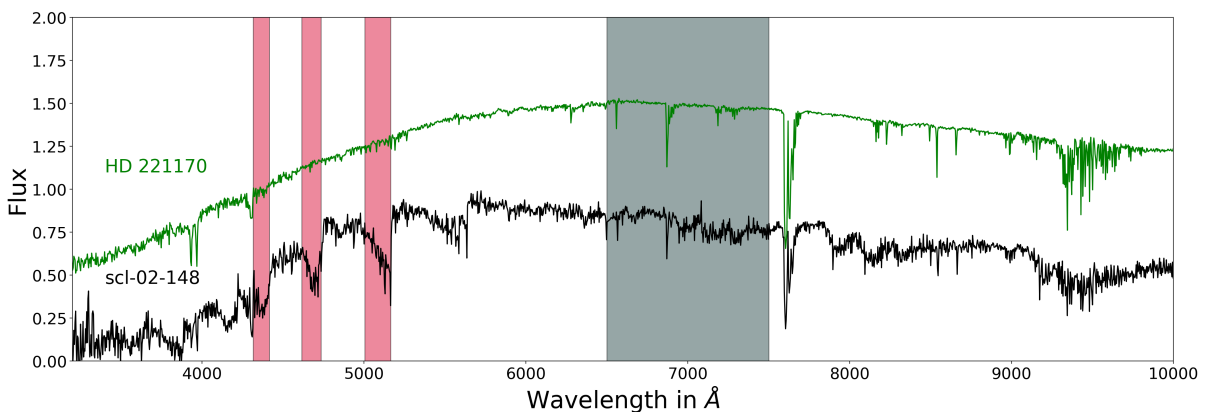

Figure 2: Comparison between a spectral type G2 star without an enhancement in carbon (HD 221170 in green) and one of the stars in this sample (scl-02-148 in black). The red shaded areas indicate regions of strong carbon absorption and the black shaded area indicates CN absorption. The spectrum of HD 22170 is taken from the X-Shooter Library Data Release 2 (Gonneau et al., 2020)). Its stellar parameters are: T_{eff} = 4591K, $\log g$ = 1.05, [Fe/H] = -2.00, from Matrozis et al. (2013). The stellar parameters of scl-02-148 are T_{eff} = 4565, $\log g$ = 1.46 and [Fe/H] = -1.73.

In Figure 2 it is clear how carbon-enhanced stars differ from normal stars in their spectrum. Especially in the bandheads of the molecular regions as shown in the shaded regions absorption is strong and the continuum is completely eaten away.

Normalizing the spectrum of a star is generally done by fitting the continuum and dividing the spectrum by this. However in C-rich stars so much of the continuum is removed by molecular absorption that it becomes a challenging task to actually find the continuum. Since these types of stars are often neglected because of their difficulty to analyze there is no standard procedure to find the continuum. I developed a method as part of this thesis to find the continuum which makes use of synthetic spectra. This was one of the major challenges of this work.

1.3.3 Measuring Abundances of Elements

The next major challenge is to measure elements whose absorption lines are affected by molecular carbon (and nitrogen) complexes, such that lines are often blended with

complex features of the molecular bands. Once again we turn to synthetic spectra to combat this. If we create a synthetic spectrum with the right abundance of carbon (and nitrogen), the synthetic spectrum will account for the blending with other lines. The challenge is to find the correct abundances of carbon and nitrogen such that we can also accurately measure other elements as well.

1.4   Sculptor Dwarf Spheroidal

By far the majority of CEMP star studies have been carried out in the Milky Way. A question one might ask is if the distribution of CEMP stars is different in different environments. Do we observe fewer CEMP-no stars in dwarf galaxies? Is there a difference in chemical composition between CEMP stars in Sculptor and our Milky Way? There are obvious differences in the evolutionary paths of these systems, but did they start out the same?

The Sculptor dwarf spheroidal galaxy is a well-studied galaxy in the Local Group. It is a satellite of the Milky Way at a distance of 86 ± 5 kpc (Pietrzyński et al., 2008) with a systemic velocity of 110.6 ± 0.5 km s^{-1} (Battaglia et al., 2008). Since Sculptor is a nearby galaxy we can observe individual red giant branch stars spectroscopically, as these stars are sufficiently bright and their spectra are relatively straightforward to analyse (e.g. Shetrone et al. (2003), Hill et al. (2019)). From colour magnitude diagram (CMD) analysis it was discovered that there was a peak in star formation about ~ 12 Gyr ago and Sculptor stopped forming stars around ~ 8 Gyr ago (de Boer et al., 2012). Sculptor consists of two distinct stellar populations, the first population is centrally located and is kinematically cold and relatively metal-rich ([Fe/H] > -1.7). The second population is more spatially extended, kinematically warmer and more metal-poor ([Fe/H] < -1.7) (Tolstoy et al., 2004).

Starkenburg et al. (2013) studied the extremely low-metallicity tail of the Sculptor dwarf spheroidal galaxy. Five of the seven stars they observed were shown to be extremely metal-poor ([Fe/H] < -3) and chemically more similar to the Milky Way halo than the more metal-rich stars in Sculptor. More recently Chiti et al. (2018) used low resolution spectroscopy (R ~ 2000) to measure the metallicity and carbon abundance of 100 stars in Sculptor and found an increase of [C/Fe] at the lowest metallicites. They measured that 24% of their sample were CEMP-no stars at [Fe/H] < -3, compared to $\sim 43\%$ in the Milky Way (Placco et al., 2014). However none of these stars have a carbon abundance of [C/Fe] > 1 compared to $\sim 32\%$ of Milky Way halo stars at [Fe/H] < -3 (Placco et al., 2014).

The most recent study of chemical abundances of Sculptor was done by Hill et al. (2019) in which they presented chemical abundances for 99 red giant branch stars. To determine the chemical abundances they made use of intermediate and high resolution spectra obtained by VLT/FLAMES. They determined many elemental abundances including s-process and r-process elements. Since this X-shooter study works with similar stars in Sculptor it will be useful to compare our work to theirs. Hill et al. (2019) concluded that their

observations are in agreement with massive stars dying as core-collapse supernovae at early times and an onset of type Ia supernovae ~ 12 Gyrs ago. Considering the scatter in neutron capture elements is low for stars with $[\text{Fe/H}] > -2.3$ it concluded that metals were typically mixed efficiently in Sculptor at later times. Lastly Sculptor shows a gradual enrichment through the r-process which is at odds with the idea of r-process events being very rare events which enrich the ISM strongly.

2 Heavy Elements

When a star lives on the main sequence it synthesises elements in its core. This process nets the star energy, allowing it to remain on the main sequence for most of its lifetime. First the star fuses hydrogen into helium through the pp chain and/or the CNO cycle. Later during a star's lifetime it fuses helium into carbon through the triple alpha process. Further helium burning consists of helium atoms fusing with carbon, oxygen and heavier elements. Fusing elements up to iron allows a massive star to delay its collapse. Elements heavier than iron have a lower binding energy per nucleon so it costs energy to fuse these. However we do find heavier elements than iron, so where do they come from?

2.1 Neutron Capture

Fusing increasingly heavy elements becomes substantially more difficult because the Coulomb barrier becomes ever stronger as the proton number increases (scales with Z^2). Creating elements heavier than iron and avoiding the Coulomb barrier completely can be done by neutron capture reactions. Since neutrons do not feel the Coulomb potential they do not have to overcome this barrier. By absorbing a neutron an isotope is created of a given element but its mass has increased by one while its proton number remains constant. Neutron-rich isotopes are often unstable and undergo β^- decay. In this process one of the neutrons is converted into a proton and an electron is ejected. The mass number of the element remains the same but its proton number increases by one. In this way it is possible to form heavier elements (Burbidge et al., 1957).

To create new elements/isotopes in this way there is a competition between the timescale of neutron capture and β^- decay, which differs for every isotope. In general there is a dichotomy in this process and these are named s-process and r-process, meaning slow and rapid neutron capture. This is usually a function of the neutron density. Finally another process is hypothesized to occur in an intermediate neutron density, the i-process (Cowan & Rose, 1977).

2.2 The s-Process

During the slow neutron capture process unstable isotopes undergo β^- decay before capturing another neutron. A consequence of this is that elements formed by the s-process will generally follow the same pathway and follow the valley of stability. A typical neutron density for the s-process is $\sim 10^8$ cm^{-3} (Beer et al. (1984) and Sneden et al. (2008)).

The s-process is thought to occur in intermediate-mass stars and takes place at the end of helium and carbon burning (Pignatari et al., 2010). Neutrons are provided when ^{22}Ne fuses into ^{25}Mg by capturing a Helium atom and releasing a neutron. This process is called the weak s-process. Another production site is thermally pulsing asymptotic giant branch (TP-AGB) stars (Bisterzo et al., 2011). In this case neutrons come from the ^{13}C to ^{16}O reaction. This process is called the main s-process.
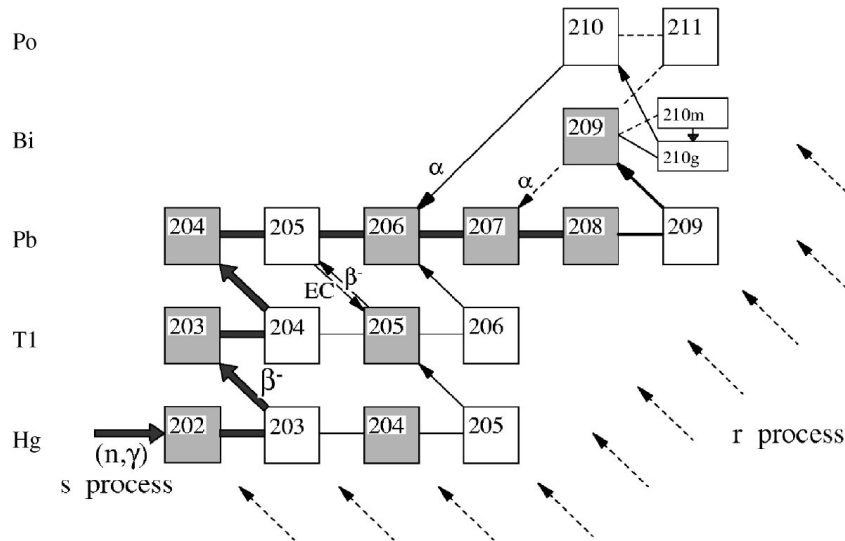
Figure 3: The termination of the s-process. Figure taken from Ratzel et al. (2004).

The s-process terminates in lead, bismuth and polonium. ^{206}Pb can capture three neutrons, then it decays into bismuth, which captures another neutron and finally decays into ^{210}Po. However, this element is unstable through alpha decay and decays into ^{206}Pb. Therefore any elements heavier than this can not be formed through the s-process (Ratzel et al., 2004).

2.3 The r-Process

For the rapid neutron capture process the density of neutrons needs to be extremely high ($> 10^{22}$ cm^{-3}), and unstable isotopes capture many more neutrons before undergoing β^- decay. When this happens isotopes further away from the valley of stability are formed (Burbidge et al., 1957).

Metal-poor stars in the Galactic halo have shown similar r-process abundance patterns to the sun (Sneden et al., 2008). This pattern appears to be robust regardless of age and metallicity. This suggests that the r-process enrichment occurred early in the chemical evolution in the Milky Way. A consequence of this is that the origin of heavy elements beyond iron seems to be well-regulated. This could be due to the nuclear properties of the r-process elements or a unique cosmic site with similar conditions generated uniformly at early cosmic time. Although the r-process pattern is relatively robust at low metallicities, there is a large scatter compared to other groups of elements such as [Eu/Fe] and [Eu/Mg]. This large scatter in [Eu/Fe] and [Eu/Mg] suggests that Eu was created in fewer and less well-mixed events compared to supernovae which create all the Mg and Fe at this metallicity.

Numerous sources have been proposed that can provide high neutron fluxes. One of them is type-II supernovae from massive stars (Burbidge et al., 1957). The collapse of the star provides an extreme neutron flux that could intake the r-process.

Another scenario is the merging of neutron stars or merging black holes. It is expected that this environment could also provide sufficiently high neutron fluxes to produce r-process enrichment (Watson et al., 2019).

2.4 The i-Process

The i-process was first hypothesized by Cowan & Rose (1977). They stated that this process might occur in evolved red giants to produce ^{14}C by capturing a neutron on a ^{14}N atom. The hypothesized neutron density is $\sim 10^{15} - 10^{17}$ cm^{-3}. In a more recent study a metal-poor main sequence star was observed with an abundance pattern from which the elements of germanium through europium could not be explained by any combination of the s- and r-process (Roederer et al., 2016). Including the i-process improved the fit of these abundances.

Dardelet et al. (2015) compared the abundance pattern in three stars with results of their nucleosynthetic simulation of the i-process. In their model they simulate one physical zone within a star with the conditions of a helium pulse-driven convective zone and a neutron density of 10^{15} cm^{-3}. Almost all of the observed heavy element abundances from yttrium to iridium are fit well in these stars as can be seen for one of the star in Figure 4. Therefore the authors concluded that the origin of heavy elements in CEMP-r/s stars could actually be from the i-process instead of a combination of r- and s-process enhancement. In a more recent study Skúladóttir et al. (2020) concluded that in order to match the observed abundances, the i-process was very likely important in the overall chemical evolution in Sculptor.
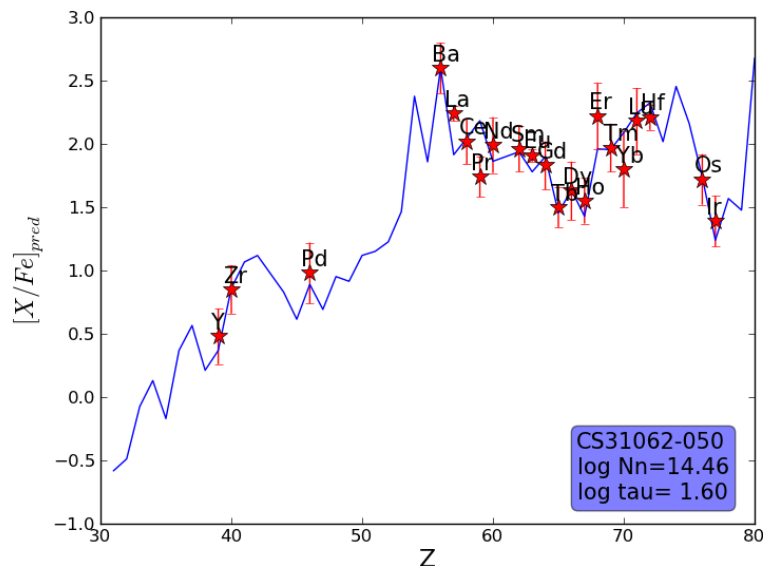

Figure 4: The best fit of the abundance pattern of the CEMP-r/s star CS 31062-050 with the i-process model (Dardelet et al., 2015). N_n is the neutron density (in cm^{-3}) and tau is the neutron exposure (in mbarn^{-1}).

3 X-shooter Observations

The motivation for the observations analysed here was the discovery of the first CEMP-no star in the Sculptor dwarf spheroidal (Skúladóttir et al., 2015). This was a surprising discovery since Sculptor appeared to be completely deficient in CEMP stars at [Fe/H] < −2 and this star was surprisingly metal-rich at [Fe/H] = −2. Extensive studies of low-metallicity stars have been made of Sculptor and none of the observed stars have been found to be carbon enhanced, for example: Tafelmeyer et al. (2010), Starkenburg et al. (2013), Kirby et al. (2015), Jablonka et al. (2015), and Simon et al. (2015).

3.1 The X-shooter Spectrograph

The X-shooter spectrograph is an instrument at the ESO Very Large Telescope (VLT) (Vernet et al., 2011). It has an intermediate resolution ($R \sim 4000 - 17000$, depending on the wavelength and slit width) and is used for single slit observations. In one exposure it covers a large spectral range, from 3000 to 25000Å. The observations are split into three arms within the instrument, the UVB arm ($3000 - 5595$Å), the VIS arm ($5595 - 10240$Å) and the NIR arm ($10240 - 24800$Å). For the purposes of our observations it is highly advantageous to work with such a large wavelength range. We knew it would be challenging to find the continuum for our stars and that it may not be well-defined as we expected large regions of absorption due to carbon and nitrogen complexes. This range also allows us to find suitable absorption lines (for example of iron) across a large wavelength range, ideally where the continuum is well-defined and there is no blending of carbon and nitrogen complexes.

3.2 Target Selection

These observations originally targeted 10 carbon-rich stars in Sculptor. Thereof 3 carbon-rich stars in Sculptor were previously identified but not analysed with VLT FLAMES surveys ((Shetrone et al., 1998), (Battaglia et al., 2008) and 7 stars from Azzopardi et al. (1985). Strong CN lines were clearly identified in these targets showing these stars to be C-rich. The observation setup used slit widths of 0.8, 0.7 and 0.9 arcsec in the UVB, VIS and IR arms respectively.

Target	RA	Dec	T_{exp} (hours)	V (mag)	Ref.
scl-03-207B	01 01 48.9	-33 31 54.2	5	19.5	1
scl-02-148	00 58 46.4	-33 41 44.3	3	18.9	2
scl-03-110	01 01 03.7	-33 37 59.0	1.5	18.3	2
Azz1	00 58 36.1	-33 40 25.8	0.75	17.5	3
Azz3	00 59 58.9	-33 28 34.3	0.75	17.7	3
Azz4	01 00 10.7	-33 40 57.5	0.75	17.5	3
Azz5	01 00 20.7	-33 45 17.7	0.75	17.4	3
Azz6	00 58 44.7	-33 30 48.9	0.75	17.7	3
Azz7	00 58 27.3	-34 01 18.4	0.75	17.4	3
Azz8	00 58 30.8	-33 28 40.0	0.75	17.5	3

Table 1: List of C-rich targets observed by X-shooter. References are as follows:
[1]Shetrone et al. (1998)
[2]Battaglia et al. (2008)
[3]Azzopardi et al. (1985).

In Figure 5 we make a comparison between our sample of stars and the sample of stars from Hill et al. (2019) on a Hertzsprung-Russell Diagram (HRD). We use the temperature as calculated by the V-J band. The sample from Hill et al. (2019) only contains stars brighter than a V-band magnitude of 18.5 since it is necessary to observe bright stars for high resolution spectroscopy.
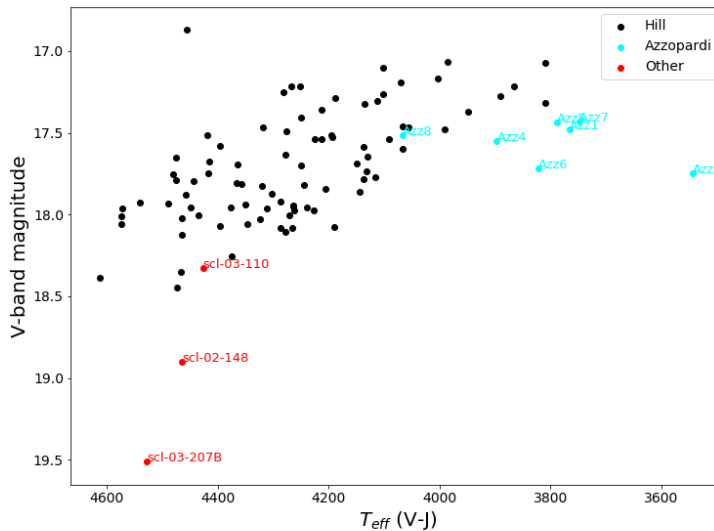

Figure 5: Comparing our sample of RGB stars in red and cyan points to the sample of Hill et al. (2019) (black points) in an HRD.

3.3 Observation Goals

The immediate goals of these observations are to make a reliable measurement of [Fe/H] and to differentiate between CEMP-s and CEMP-no stars. In our sample, 6 of the 11 stars have [Fe/H] estimates from the Ca II triplet over the range of $-3 \lesssim$ [Fe/H] $\lesssim -1.5$ (Battaglia et al., 2008). However some of these are very uncertain due to the presence of strong CN lines in the spectrum. The 8 stars from Azzopardi et al. (1985) do not have a Ca II triplet measurement of [Fe/H] as they are too C-rich. Using the large spectral range of X-Shooter we can look for iron lines throughout the stellar spectra.

Accurately measuring [Fe/H], [C/Fe] and [Ba/Fe] are the main objectives of the observations. This will allow us to categorize the stars as CEMP-s or CEMP-no stars. Another objective is where possible to measure heavier elements such as [Y/Fe], [La/Fe] and [Eu/Fe] since these help us distinguish between CEMP-s and CEMP-r stars. X-shooter will allow us to differentiate between CEMP-s and CEMP-no stars since CEMP-s stars are expected to have $\gtrsim 1.5$ dex higher [Ba/Fe] compared to CEMP-no stars. If there are stars with strong r-process enhancements we might detect the europium line at 6645Å.

4 Methodology

To analyse our sample of X-shooter observations of CEMP stars we make use of synthetic spectra rather than the more traditional approach of using equivalent widths. Synthetic spectra (when properly made) take into account not just single absorption lines but also account for blending and asymmetries in line profiles and can take into account many chemical elements simultaneously.

For synthetic spectra to be made we need to determine the stellar parameters: metallicity ([Fe/H]), effective temperature (T_{eff}), surface gravity ($\log g$) and microturbulence velocity (v_t). Then we can create a model stellar atmosphere for each star using the MARCS stellar atmosphere models (Gustafsson et al., 2008). Since the MARCS stellar atmosphere models are a grid with varying stellar parameters we interpolate between these to obtain models corresponding to our stellar parameters.

The next step is to generate a synthetic spectrum. We do this using the `TURBOSPEC` code from Plez (2012). In this program we insert the stellar atmosphere models which we created from interpolating between MARCS models given our stellar parameters, as well as atomic libraries from Kupka et al. (1999). These atomic libraries create absorption lines from our last ingredient: chemical abundances. We compare these synthetic spectra to our actual spectrum, the synthetic spectrum that matches the observed spectrum, particularly in the absorption lines or regions of interest the best gives us the chemical abundances for all elements we can identify in our spectrum.

4.1 Stellar Parameters

These parameters affect the spectrum of the stars, as well as the characteristics of absorption lines. It is required to have a good estimate of these parameters to build representative stellar atmospheres and thus representative synthetic spectra.

4.1.1 Metallicity

Metallicity is typically represented by [Fe/H] and is an important parameter in determining the properties of a stellar photosphere. Beforehand we do not know what it is for our sample of stars. However we know that generally speaking the stellar population of Sculptor is old and the peak of the metallicity distribution function lies around [Fe/H] = -2 (Starkenburg et al., 2010). This gives us a first estimate of metallicity.

4.1.2 Effective Temperature

The effective temperature (T_{eff}) of a star is the temperature of a blackbody that emits the same amount of electromagnetic radiation as emitted by the star, $F_{\mathrm{bol}} = \sigma T_{\mathrm{eff}}^4$. The T_{eff} of a star can be determined with the Infrared flux method (IFRM), developed by Blackwell & Shallis (1977), which uses the fraction of flux in the IR and compares this to models to find the best fit for T_{eff}. Since this method is very time consuming we use an empirical relation derived from this method which calculates T_{eff} from the photometric colours (Ramírez & Meléndez, 2005):

$$T_{\text{eff}} = \frac{5040}{\theta_{\text{eff}}} + P(X, [\text{Fe/H}]) \tag{4.1}$$

where

$$\theta_{\text{eff}} = a_0 + a_1 X + a_2 X^2 + a_3 X[\text{Fe/H}] + a_4[\text{Fe/H}] + a_5[\text{Fe/H}]^2. \tag{4.2}$$

Where a_i are the coefficients of the fit, which are calculated for different colours and dwarf and giant stars, X represents the colour of the star and P is a polynomial of the following form: $\sum_{i=0}^{5} P_i x^i$. Both coefficients a and P are calculated in Ramírez & Meléndez (2005).

We have photometry in numerous photometric bands for our sample of stars. Since our stars contain regions with very high carbon absorption this will affect the colour measure. We will calculate the colour between different bands and compare these to normal stars to investigate which bands are most suitable for the effective temperature determination.

4.1.3   Surface Gravity

The surface gravity g is defined as the gravitational acceleration at the surface of the star: $g = \frac{GM}{R^2}$. It is often expressed in a base 10 logarithm ($\log g$). Since we know the distance to our stars (as they are all in the Sculptor dwarf spheroidal), we can calculate the absolute bolometric magnitude (M_{bol}). From that we calculate the surface gravity as follows:

$$\log g = \log g_{\odot} + \log \frac{M}{M_{\odot}} + 4\log \frac{T_{\text{eff}}}{T_{\text{eff},\odot}} + 0.4(M_{\text{bol}} - M_{\text{bol},\odot}). \tag{4.3}$$

Where M is the mass of the star. The solar value is denoted by the subscripted $\odot$.

4.1.4   Microturbulence Velocity

Microturbulence velocity can cause broadening of absorption lines in the spectrum, for giant stars it can be calculated in the following way (from Kirby et al. (2009)):

$$v_t = 2.70 - 0.51 \log g. \tag{4.4}$$

4.2   Synthetic Spectra

Measuring the abundances of stars is often done by using equivalent widths of absorption lines. Problems can arise when using this method if there are multiple lines or absorption regions which overlap. Our strategy of abundance measurements makes use of synthetic spectra to be able to accurately account for blends. By comparing the synthetic spectra to our observed spectrum we find the abundance measurement by taking the best fit for the absorption lines or regions.

We use the program TURBOSPEC to generate synthetic spectra which is made by Alvarez & Plez (1998). Creating the synthetic spectra requires the following: a stellar

atmosphere model and an initial guess for the abundances we are interested in. To measure the abundance we create a grid of models around the initial guess we have for a star. In this grid we vary the abundances of the different elements one at a time. With the best fits we create a new best guess of abundances and create another grid of models around this model. This process is repeated iteratively until the abundance measurements converge. These last abundances are our final measurements for the star.

4.2.1 Stellar Atmosphere Models

Stellar atmospheres are taken from MARCS (Gustafsson et al., 2008), which are 1D, LTE models. However these stellar atmospheres do not perfectly match to our stars, so we interpolate between a number of models to create a stellar atmosphere given our values of temperature, metallicity and surface gravity.

4.2.2 Line Lists

When measuring abundances we make use of line lists to measure every element we are interested in. Which lines are suitable depends on the stellar parameters, spectral resolution and the wavelength coverage of the spectrum. Many line lists for different types of stars can be found in the literature but in this research we investigated and built our own line list. Since we are making use of synthetic spectra we can use these to find suitable absorption lines. We do this by creating multiple synthetic spectra, in which the only difference is the absence of one element. The difference in these spectra reveals where absorption lines can be expected to be found and how much they will blend with other lines. Ideally these lines are strong and not blended with other lines. An example of a barium line is shown in Figure 6.
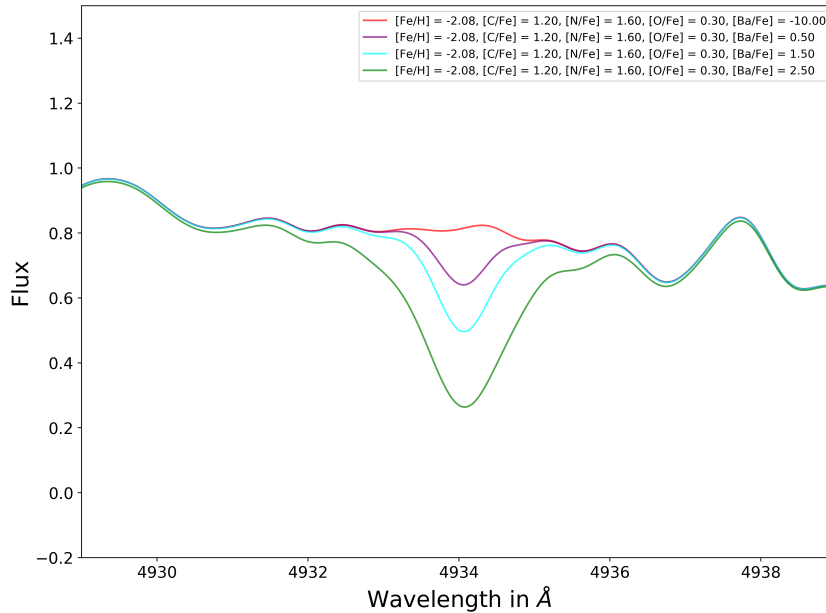
Figure 6: Four synthetic spectra for a given C, N and O abundance differing only in [Ba/Fe]. The red curve represents the star in the complete absence of barium while the other curves represent increasing abundances of barium (see legend). The synthetic spectra have been convolved to match the resolution of our X-shooter spectra.

For most elements, such as iron, we end up with a line list with a number of absorption lines. Our line list can be found in Appendix A. However, carbon and nitrogen molecules cover very large regions of the spectrum in complex absorption line complexes as shown in Figure 2. To measure these we find regions in which there is sensitivity to changes in the abundances of carbon and nitrogen. Then our line list consists of 10Å segments across these regions.

4.3 Continuum Normalization

Synthetic spectra are normalized, this means that at points where there are no absorption lines the flux value is 1. If stellar spectra are not normalized, in general they behave like blackbodies and have a spectrum which follows Planck's Law. To account for this we have to normalize the observed spectrum, to create a flat continuum.

To do this we have to develop a method to find the continuum in our observed spectra covered in carbon and nitrogen molecular line complexes. In general this is not a difficult task when you have a blackbody profile with a number of atomic absorption lines. However, due to the molecular line complexes there are large regions of absorption throughout the spectrum. This makes it difficult to locate the true continuum level.

The first step we do is remove regions that contain telluric absorption according to Rudolf et al. (2016). To account for cosmic rays and outliers we calculate a rolling median for every point in the observed spectrum and and remove all points which are more than 0.5 standard deviation higher than this rolling median (see Figure 7a).

We make use of a synthetic spectrum for the star to help locate regions of continuum (see Figure 7b). If the flux value of the synthetic spectrum is equal to 1 we take the observed flux value as a continuum point. However it turns out that for carbon enhanced stars often there are simply no regions of continuum for large parts of the spectrum. Therefore we make use of a lower flux value to find continuum. In the case of scl-02-148 we identify all points in the synthetic spectrum which are above 0.85. We use these points to estimate where we we would expect near-continuum points in the real spectrum. We do this by dividing the observation by the value of the synthetic spectrum.
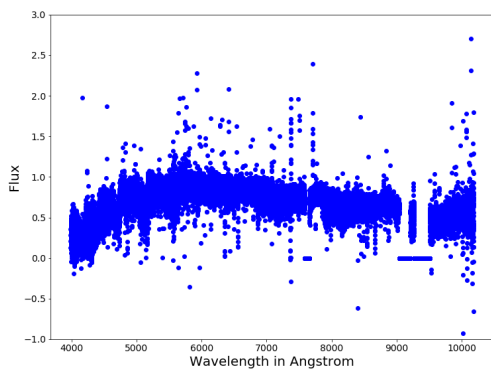
(a) Raw co-added spectrum.
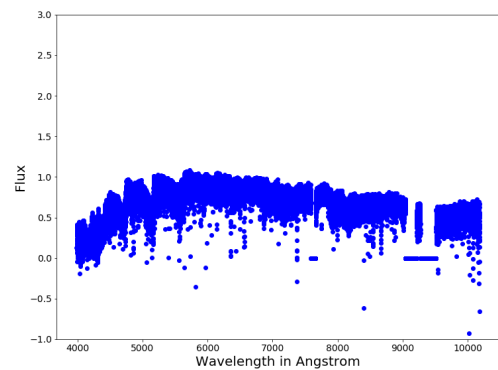
(b) Clipped spectrum.
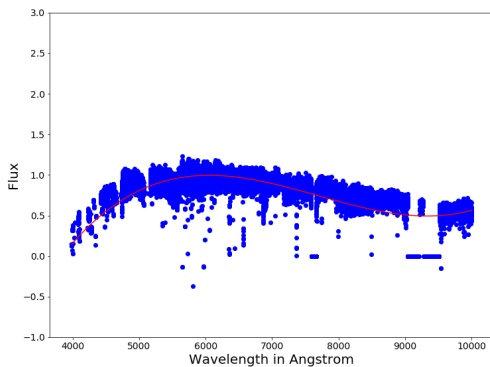
(c) Fit through points after clipping and se-
lecting points making use of a synthetic spec-
trum.
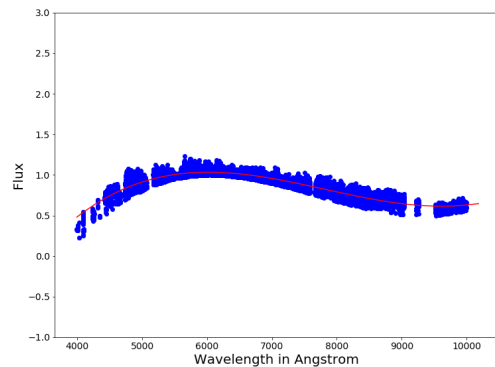
(d) A fit through the continuum points.

Figure 7: Determination of the continuum fit of scl-02-148.

We create a fit through these points and remove all points lower than this fit (see figure 7c). This is an effort to best trace the continuum. The last step is to create a fit through these continuum points and interpolate to cover all wavelengths we are interested in (see figure 7d). Then we can divide our observed spectrum by this continuum in order to obtain the normalized spectrum (Figure 8).
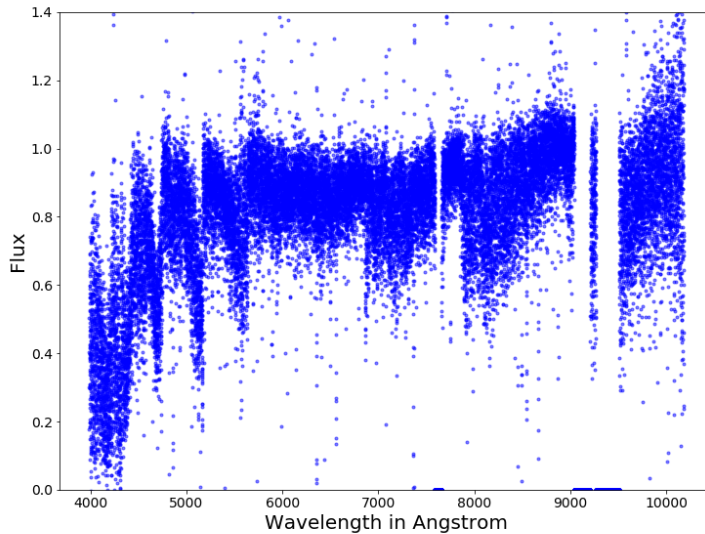
Figure 8: The resulting normalized spectrum of scl-02-148.

4.4 Abundance Measurements

For abundance measurements we make use of the line lists we have created for all elements we are interested in. This line list can be found in Appendix A. For each element we create a grid of synthetic spectra in which we only vary the single element we are measuring. Then for each absorption line or region we calculate the χ^2 statistic for each spectrum in the grid. We can interpolate a curve through these points, the minimum χ^2 reveals the preferred abundance.

Since we have to start with a base model we first start out with initial guesses of abundances. After measuring the elements we are interested in we create a new base model from which we iterate our measurements. This is important since this synthetic spectrum is used for continuum normalization, which will be different once we update the synthetic spectrum. Furthermore measurements of one element can be dependant on another element, especially in regions with blending. This process is done iteratively until the measured abundances are stable and we have the final measurements for the star.

4.4.1 Solar Abundances

All models and measurements are done in a system in which we compare abundances against solar abundances (for example [C/Fe] = 1.0 means that the ratio of carbon over iron is 10 times as high compared to the Sun). Therefore it is important to quantify which solar abundances we use. For consistency with other studies done on Sculptor we adopt solar abundances from Grevesse & Sauval (1998).

5 Results

5.1 Stellar Parameters

The temperatures of our stars are determined from photometric magnitudes as described in Section 4.1.2. Since photometry is affected by the strong regions of absorption we compare our measurements to Hill et al. (2019). They also observed red giants in the Sculptor dwarf spheroidal but they omitted C-rich stars. The aim of this comparison is to choose a combination of photometric bands which are suitable for determining T_{eff}. The comparisons can be seen in Figure 9, where we determine that the (V-J) and (V-K) bands are the most suitable for temperature determination since the scatter is lowest and all C-rich stars show the least offset.
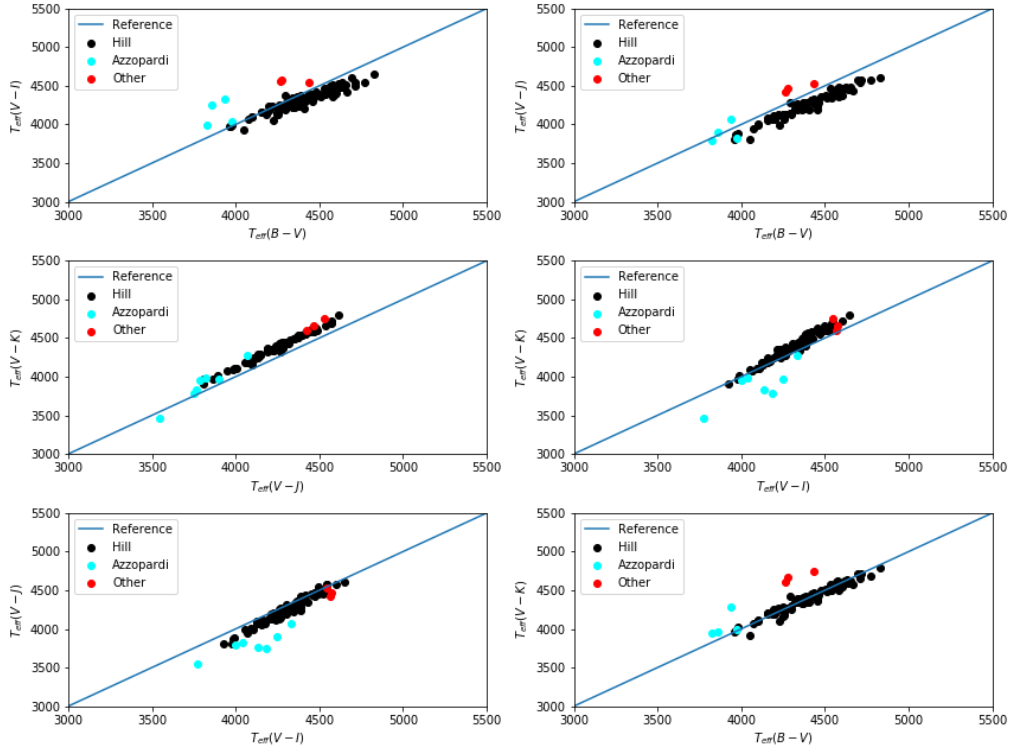
Figure 9: Comparison of temperature calculations by combinations of different photometric bands. The blue reference line indicates a perfect correlation, the black points are measurements from Hill et al. (2019), the cyan and red points are from this work. Cyan points indicate the Azzopardi stars and the red points indicate the scl-02-148, scl-03-110 and scl-03-207B.
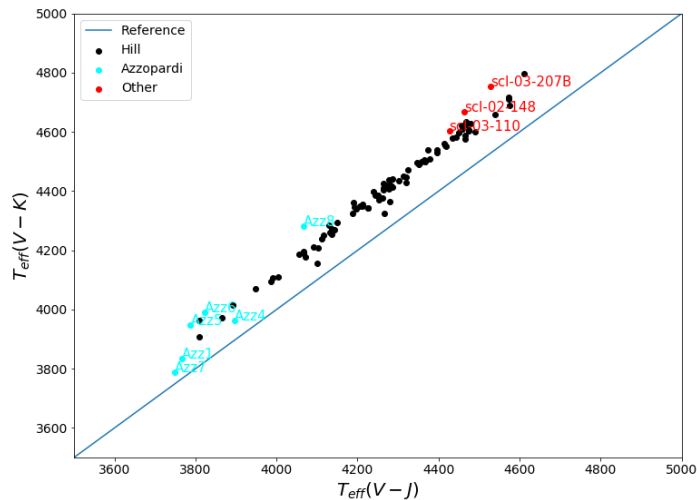
Figure 10: The chosen bands for determining temperature, colours are the same as in Figure 9 and our sample are identified.

The temperature is determined by using Equation 4.1 and we assume [Fe/H] = −1.8. Then we calculate the surface gravity and microturbulence velocity with Equations 4.3 and 4.4 respectively. The results can be found in Table 2.

Name	T_{eff} (K)	log g	v_{mic} (km s^{-1})	V (mag)	V-J (mag)	V-K (mag)
scl-02-148	4565	1.46	1.96	18.901	2.002	2.461
scl-03-110	4515	1.20	2.09	18.327	2.040	2.535
scl-03-207B	4640	1.75	1.81	19.509	1.941	2.366
Azz1	3799	0.28	2.56	17.481	2.889	3.743
Azz3	3499	-0.15	2.76	17.750	4.376	5.384
Azz4	3929	0.47	2.46	17.548	2.633	3.450
Azz5	3867	0.31	2.54	17.437	2.841	3.484
Azz6	3906	0.47	2.46	17.718	2.770	3.393
Azz7	3768	0.23	2.58	17.440	2.930	3.860
Azz8	4174	0.65	2.37	17.514	2.375	2.898

Table 2: Stellar parameters and photometric bands of our sample.

The methodology discussed in Section 4 proved to be insufficient for the Azzopardi stars. Absorption regions from carbon and nitrogen were too strong in these stars to successfully estimate a continuum. A comparison of a number of Azzopardi stars with a carbon normal star and one of our other stars is shown in Figure 11. It is clear that the absorption regions (shown in the shaded areas) present in scl-02-148 are even more extreme in the Azzopardi stars. The abundances of carbon and nitrogen are obviously extremely high. Combining this with the fact that molecular absorption is stronger in lower temperature stars makes these stars incredibly challenging to analyse. Therefore from this point onward we analyse only these 3 stars: scl-02-148, scl-03-110 and scl-03-207B. Furthermore we omit the IR

arm observations, this is done since synthetic spectra are most reliable for the UV/VIS arm observations. We also can perform the measurements of elements we are interested in with only the UV/VIS arm observations.
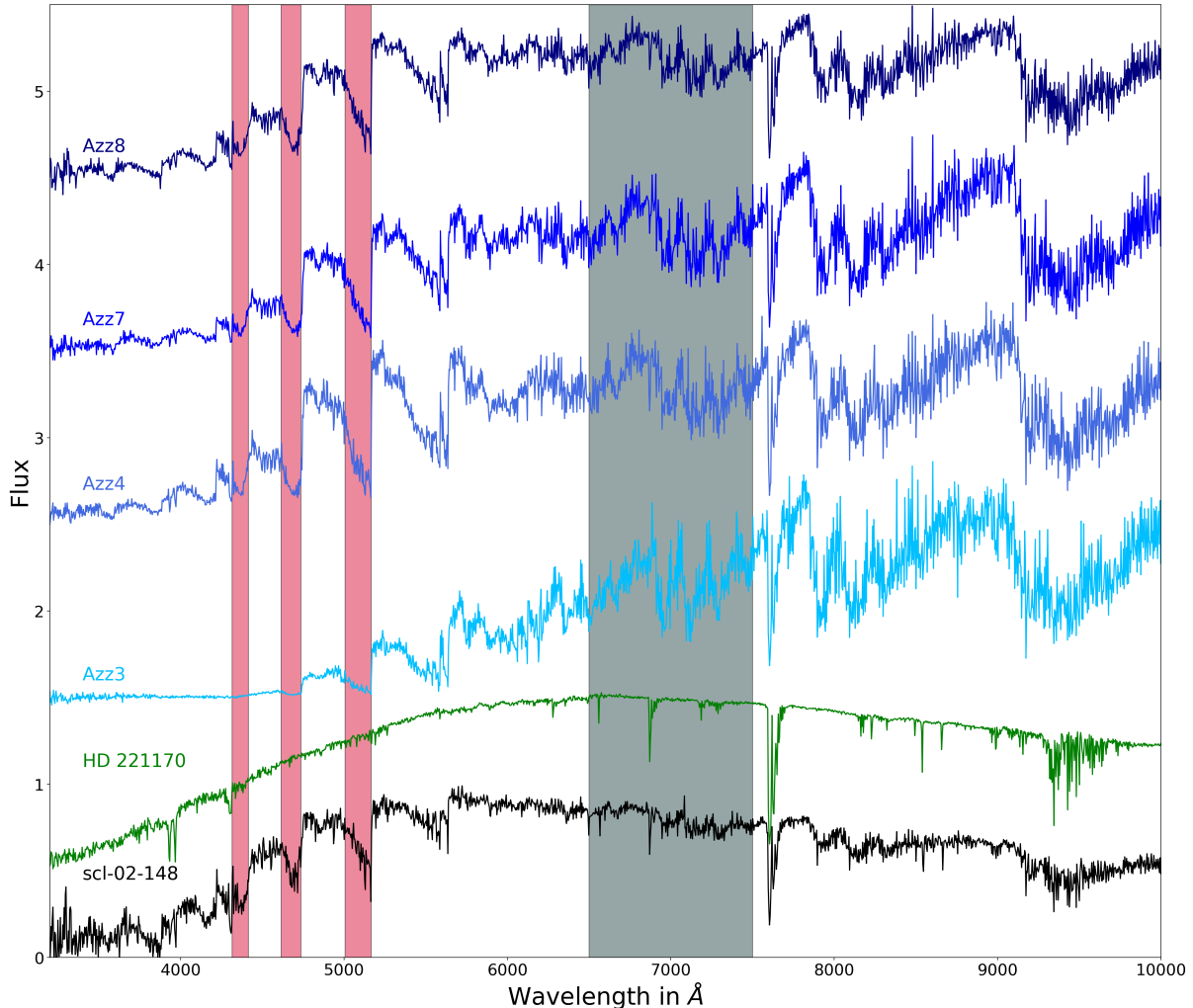

Figure 11: A comparison between the spectra of a number of Azzopardi stars (in different shades of blue) with a carbon normal star (HD 221170 in green) and one of our other stars (scl-02-148 in black). The red shaded area indicates the bandheads of carbon, the black shaded area indicates an absorption region of CN. The stellar parameters of HD 221170 are: T_{eff} = 4591K, $\log g$ = 1.05, [Fe/H] = -2.00, from Matrozis et al. (2013). Stellar parameters of the Azzopardi stars and scl-02-148 are shown in Table 2.

5.2 Abundance Measurements

Carbon and nitrogen in these C-rich stars have a large impact on the overall spectrum. Since we are making use of synthetic spectra to estimate the continuum we iteratively measure these elements until we have a synthetic spectrum which matches our observations the best. For these elements a line list was made as discussed in Section 4.2.2. For carbon and nitrogen large regions of the spectrum were sensitive to change in the abundance. Additionally, we tested these elements on the strength of this sensitivity. Carbon

turns out to be most sensitive to change in the bandheads of absorption regions. These regions are the following: $4315 - 4415$Å (CH), $4615 - 4735$Å (CH) and $5005 - 5165$Å (C$_2$). These regions are used to measure the abundances of carbon. Sensitivity in nitrogen is strongest in regions with CN molecular absorption ($\sim 6400 - 9400$Å). This sensitivity is relatively constant throughout this wavelength range, we measure nitrogen from $6500 - 7500$Å. The carbon bandheads and CN regions are shown as shaded regions in Figure 11. We include iron lines we found in the range of $4600 - 5400$Å as these suffered the least blends.

As a test for our continuum determination we inspect the measurements of iron, carbon and nitrogen over their respective wavelength ranges. If there is no trend in the measured abundances with wavelength this confirms that the continuum is determined correctly.

The complete line list for all elements (excluding carbon and nitrogen) can be found in Appendix A. The absorption lines varied in quality among our stars, care was taken to only include measurements which have errorbars within the grid of models. This grid typically spans two dex. Furthermore a visual check was done to ensure the continuum was determined sufficiently well around that area and that we are not just measuring noise.

5.2.1 Iron

The iron lines in our line list span from ~ 4600Å to ~ 5400Å, and in total 16 lines were identified. We did not to choose to include absorption lines within bandheads of carbon regions since these lines would be very challenging to measure. An example of an absorption line, alongside synthetic spectra is shown in Figure 12.
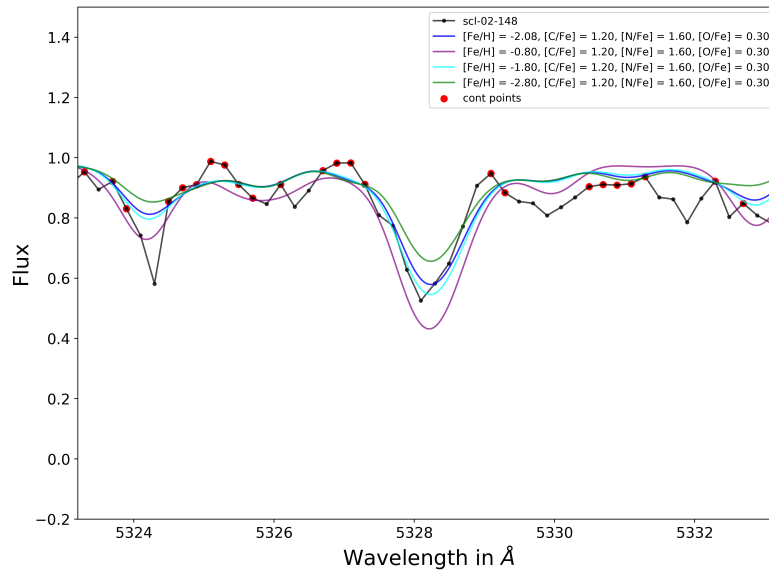
Figure 12: For scl-02-148 the iron absorption line at 5328Å is shown. In black we have the observed spectrum, while synthetic spectra are plotted in various colours (see legend). The blue model is the fiducial model used for determining the continuum, while the other colours have different iron abundances. Red points indicate points which were used for continuum determination.

Abundance measurements of all iron lines can be found in Figure 13. In this figure all iron measurements are plotted as a function of wavelength for all stars. In none of these figures there is an obvious trend of [Fe/H] as a function of wavelength.
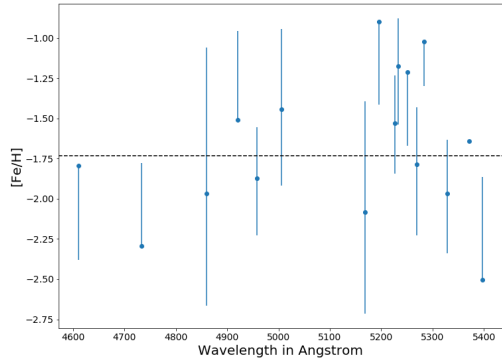
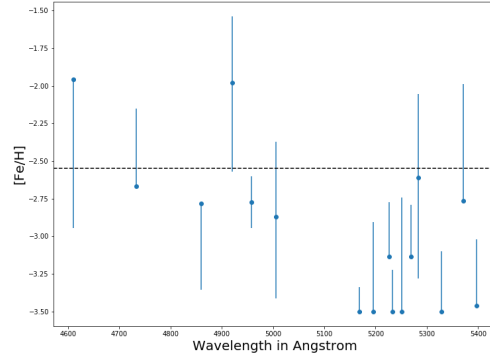(a) scl-02-148, [Fe/H] $= -1.73 \pm 0.16$.
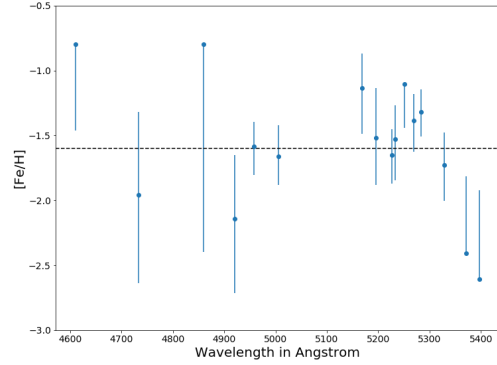
(b) scl-03-110, [Fe/H] $= -1.60 \pm 0.15$.

(c) scl-03-207B, [Fe/H] $= -2.55^{+0.42}_{-0.49}$.

Figure 13: Measured [Fe/H] as a function of wavelength for all stars. A lack of errorbar indicates an error larger than the grid allows. Only measurements with errorbars on both sides were used to calculate [Fe/H]. Note that the y-axis is different among the stars.

5.2.2 Carbon

[C/Fe] is determined in the following regions: $4315 - 4415$Å, $4615 - 4735$Å and $5005 - 5165$Å with intervals of 10 Å. These regions are the bandheads of carbon regions. The exception to this is scl-03-207B, for this star we did not include the $4315 - 4415$Å region. This region was not consistent with the other two regions and had considerably larger errorbars. This is likely due to the fact that the continuum is poorly defined in this region. The measurements are shown in Figure 14. Note that measurements were also done surrounding the bandheads. It is clear that even though the spectrum is sensitive to changes in carbon in these regions, errors are large and measurements are not always consistent.
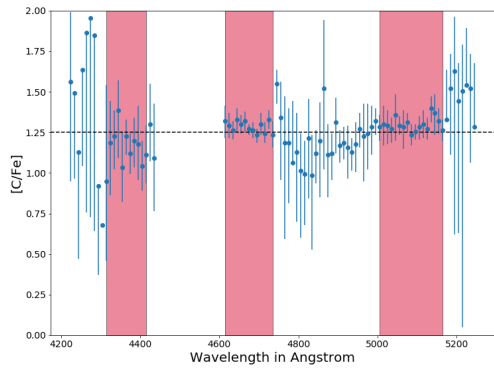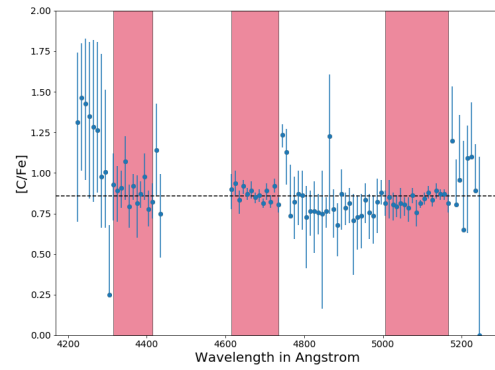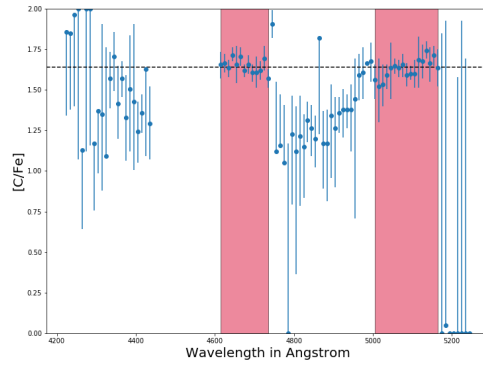
(a) scl-02-148, $[C/Fe] = 1.25 \pm 0.03$.

(b) scl-03-110, $[C/Fe] = 0.86 \pm 0.03$.

(c) scl-03-207B, $[C/Fe] = 1.64 \pm 0.09$.

Figure 14: Measured [C/Fe] as a function of wavelength for all stars. A lack of errorbar indicates an error larger than the grid allows. Only measurements in the bandheads (shaded regions) were taken into account to calculate [C/Fe].

5.2.3 Nitrogen

Nitrogen was measured in the region $6500-7500\text{Å}$ for all stars in steps of 10Å as indicated with a shaded region in Figure 11. The measurements are shown in Figure 15.
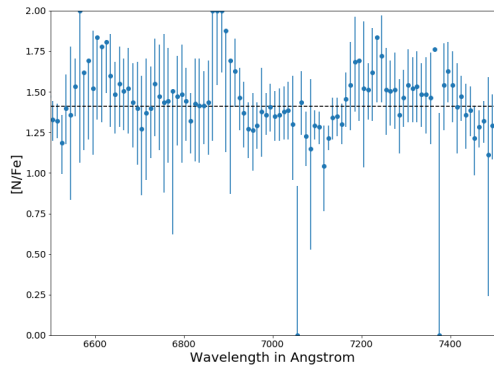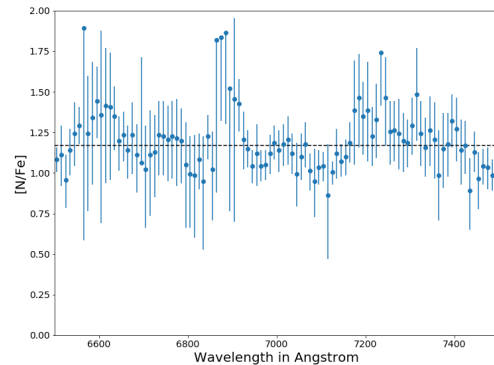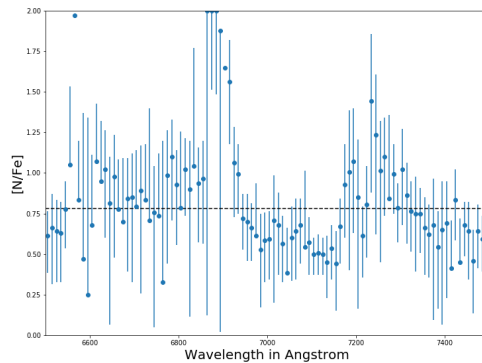
(a) scl-02-148, [N/Fe] = 1.41 ± 0.04.

(b) scl-03-110, [N/Fe] = 1.17 ± 0.05.

(c) scl-03-207B, [N/Fe] = 0.78 ± 0.08.

Figure 15: Measured [N/Fe] as a function of wavelength for all stars. A lack of errorbar indicates an error larger than the grid allows.

5.2.4 Barium

For [Ba/Fe] there are 4 available absorption lines. The bluest line (4934Å) suffers many complications. First of all it is blended, hyperfine splitting needs to be taken into account and this line likely suffers from NLTE effects (Gallagher et al., 2010). In our measurements it is generally not consistent with the redder lines. Therefore we do report the measurement this line gives but do not take it into account for measuring [Ba/Fe] in all stars. In Figure 16 the 4 lines are shown of scl-03-110 as well as the 2 lines of scl-03-207B which give a measurement. Both stars are shown since their abundances are very different.

(a) scl-03-110, [Ba/Fe] = $1.51^{+0.13}_{-0.15}$.

(b) scl-03-110, [Ba/Fe] = $2.13^{+0.23}_{-0.18}$.

(c) scl-03-110, [Ba/Fe] = $1.83^{+0.14}_{-0.16}$.

(d) scl-03-110, [Ba/Fe] = $2.01^{+0.10}_{-0.09}$.

(e) scl-03-110, [Ba/Fe] = $0.44^{+0.35}_{-0.04}$.

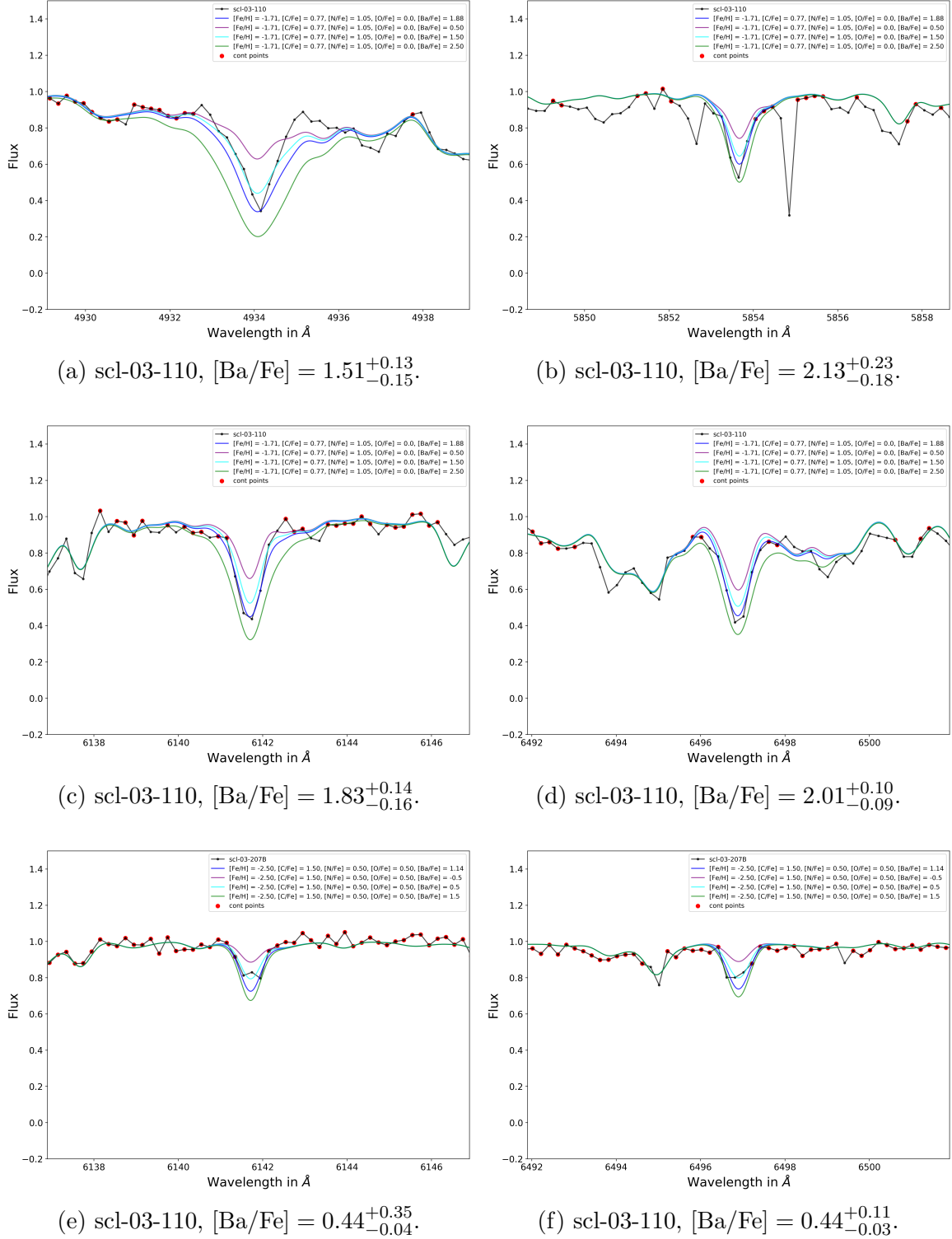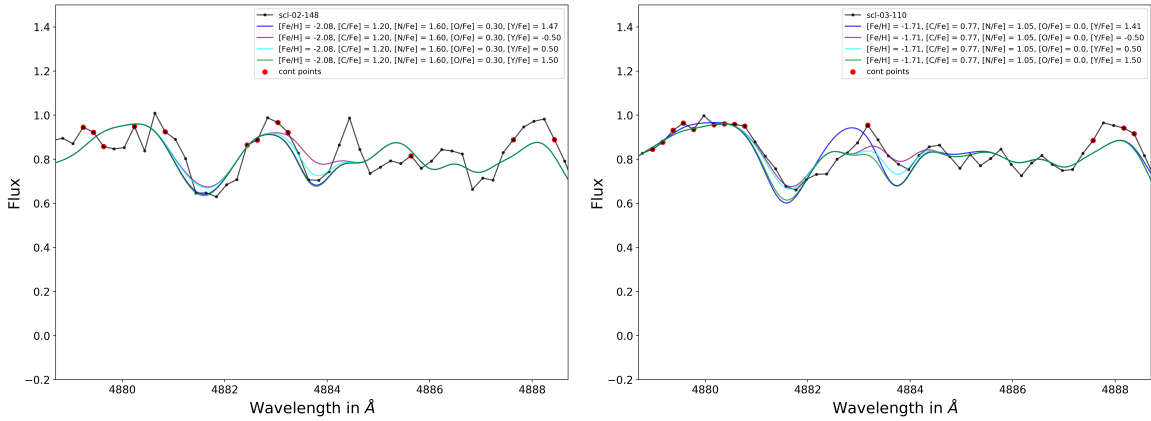(f) scl-03-110, [Ba/Fe] = $0.44^{+0.11}_{-0.03}$.

Figure 16: Barium lines for scl-03-110 and scl-03-207B. In black we have the observed spectrum, while synthetic spectra are plotted in various colours for different abundances (see legend). The blue model is the fiducial model used for determining the continuum, while the other colours have different [Ba/Fe]. Red points indicate points which were used for continuum determination.

5.2.5 Yttrium

Three yttrium lines were identified in the spectra our of stars. However two of these lines are known to be blended with other absorption lines (Hinkle et al., 2000). The absorption line at 4900Å is blended with titanium as well as barium. The line at 5205Å is blended with an iron and a chromium line. We choose to show the measurements of the line at 4883Å for all stars (Figure 17). Unfortunately for scl-03-207B at the point of the absorption line we detected a cosmic ray so this line cannot be used. The other measurements are reported in Appendix B for completeness.

(a) scl-02-148, [Y/Fe] = 0.66 ± 0.63.

(b) scl-03-110, [Y/Fe] < 0.00.
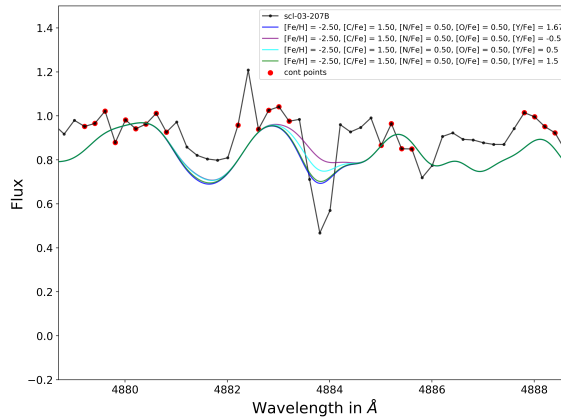
(c) scl-03-207B, no measurement.

Figure 17: Yttrium lines for all stars. In black we have the observed spectrum, while synthetic spectra are plotted in various colours for different abundances (see legend). The blue model is the fiducial model used for determining the continuum, while the other colours have different [Y/Fe]. Red points indicate points which were used for continuum determination.

5.2.6 Lanthanum

Since we have 10 lanthanum lines in the line list we only choose to show a few lines of scl-02-148 here. All absorption lines in Figure 18 have a measurement and errors within the

synthetic grid. Both scl-02-148 and scl-03-110 have measurements while for scl-03-207B we can only give an upper limit.

(a) scl-02-148, $[La/Fe] = 3.09^{+0.21}_{-0.22}$.

(b) scl-02-148, $[La/Fe] = 2.52^{+0.35}_{-0.37}$.

(c) scl-02-148, $[La/Fe] = 2.68^{+0.34}_{-0.35}$.

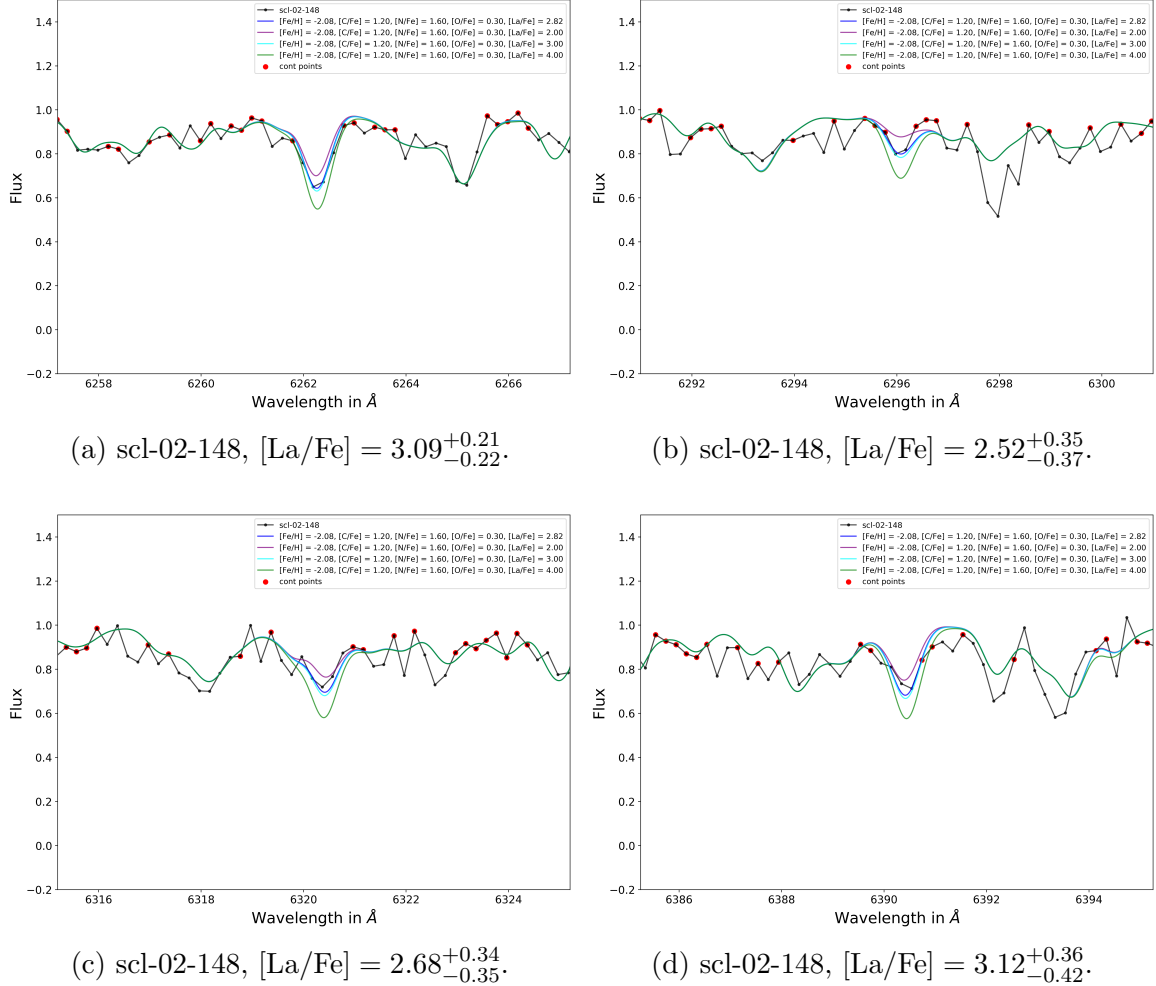(d) scl-02-148, $[La/Fe] = 3.12^{+0.36}_{-0.42}$.

Figure 18: Lanthanum lines for scl-02-148. In black we have the observed spectrum, while synthetic spectra are plotted in various colours for different abundances (see legend). The blue model is the fiducial model used for determining the continuum, while the other colours have different [La/Fe]. Red points indicate points which were used for continuum determination.

5.2.7   Neodymium

In our spectra 7 neodymium lines were identified, most of them are known to be blended (Hinkle et al., 2000). Because of this we have a large spread in measurements of [Nd/Fe]. We choose to show two lines of scl-03-110 in Figure 19 that are not heavily blended. For scl-03-207B none of the lines are strong enough to measure [Nd/Fe]. Therefore we determine an upper limit using the lines which give a measurement for scl-02-148 and scl-03-110.

(a) scl-03-110, [Nd/Fe]$2.18^{+0.18}_{-0.20}$.

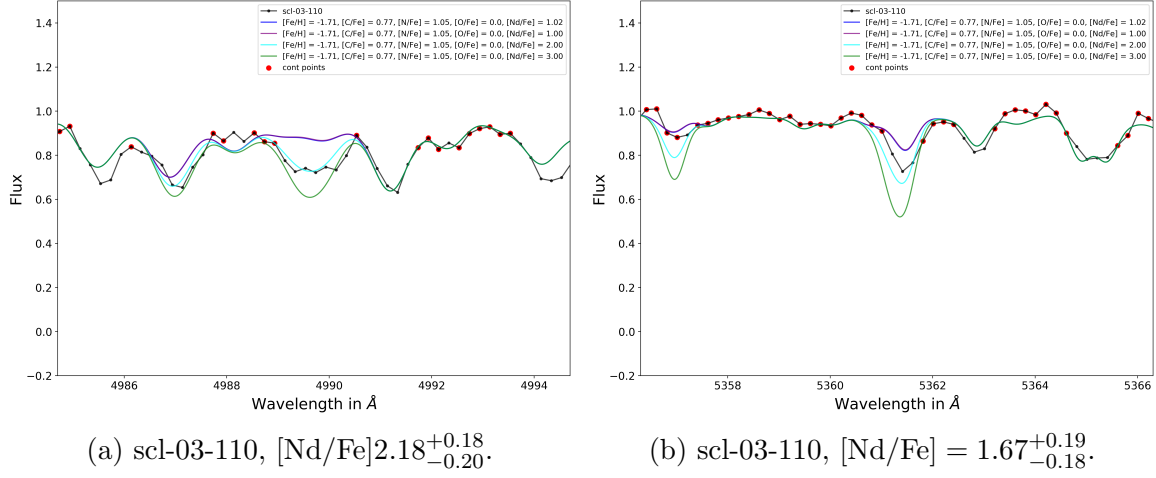(b) scl-03-110, [Nd/Fe] $= 1.67^{+0.19}_{-0.18}$.

Figure 19: Neodymium lines for scl-03-110. In black we have the observed spectrum, while synthetic spectra are plotted in various colours for different abundances (see legend). The blue model is the fiducial model used for determining the continuum, while the other colours have different [Nd/Fe]. Red points indicate points which were used for continuum determination.

5.2.8 Europium

For europium we only have a single absorption line and this is a weak line so we can only determine an upper limit for our stars. The lines with their upper limits are shown in Figure 20.
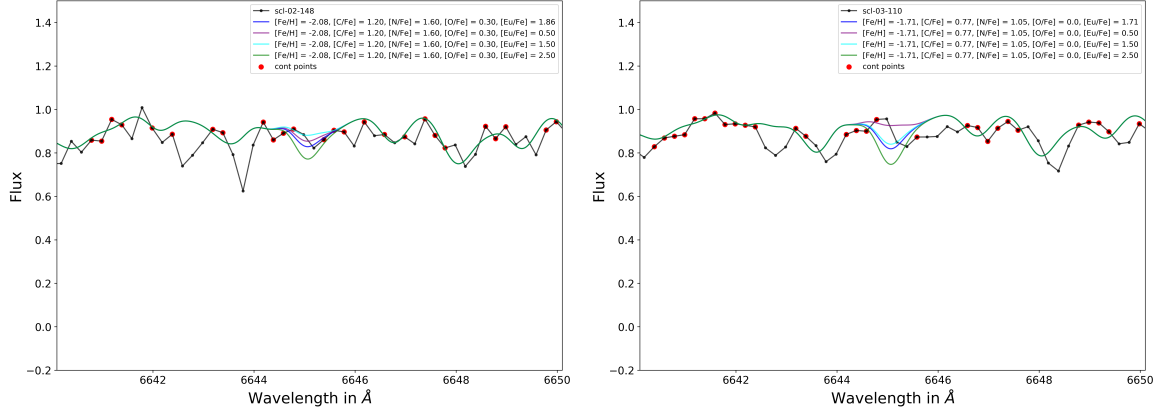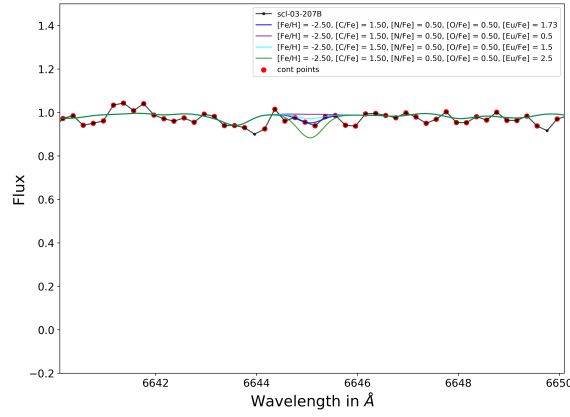
(a) scl-02-148, [Eu/Fe] $\leq$ 2.50.

(b) scl-03-110, [Eu/Fe] $\leq$ 2.50.

(c) scl-03-207B, [Eu/Fe] $\leq$ 2.50.

Figure 20: The europium line for all stars. In black we have the observed spectrum, while synthetic spectra are plotted in various colours for different abundances (see legend). The blue model is the fiducial model used for determining the continuum, while the other colours have different [Eu/Fe]. Red points indicate points which were used for continuum determination.

5.2.9 Total Abundance Measurements

In Table 3 the averaged abundance measurements (or upper limits) for all stars can be found. Individual measurements for iron and the neutron capture elements can be found in Appendix B. Error determination is described in Section 5.3.

	scl-02-148	scl-03-110	scl-03-207B
[Fe/H]	-1.73 ± 0.16	-1.60 ± 0.15	$-2.55^{+0.42}_{-0.49}$
[C/Fe]	1.25 ± 0.03	0.86 ± 0.03	1.64 ± 0.09
[N/Fe]	1.41 ± 0.04	1.17 ± 0.05	0.78 ± 0.08
[Y/Fe]	0.66 ± 0.63	≤ 0.00	$-$
[Ba/Fe]	$2.15^{+0.19}_{-0.35}$	$1.99^{+0.14}_{-0.17}$	$0.44^{+0.23}_{-0.04}$
[La/Fe]	2.78 ± 0.16	$2.75^{+0.34}_{-0.37}$	≤ 2.00
[Nd/Fe]	$2.29^{+0.40}_{-0.43}$	1.96 ± 0.26	≤ 2.00
[Eu/Fe]	≤ 2.50	≤ 2.50	≤ 2.50

Table 3: Measured abundances of our sample of stars.

5.3   Error Determination

As described in Section 4.4 we measure abundances of individual lines at the minimum χ^2. For estimating the error of an individual line we inspected synthetic spectra of iron lines. We determined that multiplying the minimum of this curve by 1.25 is the limit of a reasonable synthetic spectrum. The models which correspond to this value we take as the upper and lower limit of our measurement. For elements where we have four or fewer measured lines we take the error of our measurement to be the average of these errors. For elements with five or more measured lines we calculate the error from the scatter of measurements:

$$\delta = \frac{\sigma}{\sqrt{N}}. \tag{5.1}$$

6 Interpretation

To put our results in context we compare our stars to both Milky Way stars and other stars in the Sculptor dwarf spheroidal. To ensure we compare our sample to suitable stars we only compare them to stars with low metallicities. The comparison is shown in Figure 21. First we observe that our 3 stars are generally quite different from the general population of both Milky Way and Sculptor stars. It is clear that these CEMP stars stand out. Scl-03-110 and scl-02-148 are very similar in most of their abundances while scl-03-207B is evidently different. Since our stars are so different from the general population we also compare them to 3 peculiar stars found in Sculptor as well as a unique Milky Way star.

Scl-03-110 and scl-02-148 show some similarities to the s-process rich star found by Geisler et al. (2005) (the cyan diamond at [Fe/H] = -0.97). In [Ba/Fe] these stars are very similar, while in [Y/Fe] the Geisler star is more abundant while our stars are more abundant in [La/Fe]. Unfortunately the Geisler star does not have measurement in [C/Fe], but this star was excluded from the analysis of Hill et al. (2019) because of high CN molecular absorption in its spectra. The Geisler star is therefore likely to be C-enhanced. In Skúladóttir et al. (2020) the Geisler star was compared to theoretical models and it was found that its abundance pattern was best matched with a model of the i-process from Hampel et al. (2016). No satisfactory match was found to pure s-process or r-process models. Perhaps our stars, scl-02-148 and scl-03-110 are a more metal-poor counterpart to this star? Could their enhancement also have been caused by the i-process?

In our large comparison with metal-poor stars from Roederer et al. (2014) there are no stars with similar enhancements in [La/Fe] and [Nd/Fe] as scl-02-148 and scl-03-110 we consulted the SAGA (Stellar Abundances for Galactic Archaeology) database for similar stars. One star found by Goswami et al. (2006) was classified as a CEMP-r/s star and has very similar abundances to our stars. It is slightly more metal-poor and more enriched in [C/Fe] but is strikingly similar in [Ba/Fe], [La/Fe] and [Nd/Fe]. This star is enriched through the r-process with an abundance of [Eu/Fe] = 1.97, however our spectra are insufficient to exclude whether our stars are enhanced to a similar level and we could only determine an upper limit.

Scl-02-148 and scl-03-110 are both enriched in [C/Fe] and [Ba/Fe] as well as other s-process elements. It is unlikely that these stars are highly enriched in r-process elements since we only find an upper limit for [Eu/Fe]. Following the definition of Beers & Christlieb (2005) as shown in Section 1.2 we classify these stars as CEMP-s stars. This means that these stars have obtained their enhancement in carbon and s-process elements due to mass transfer with a binary companion. However we do not have enough radial velocity measurements of these stars to confirm whether these stars live in binary systems.
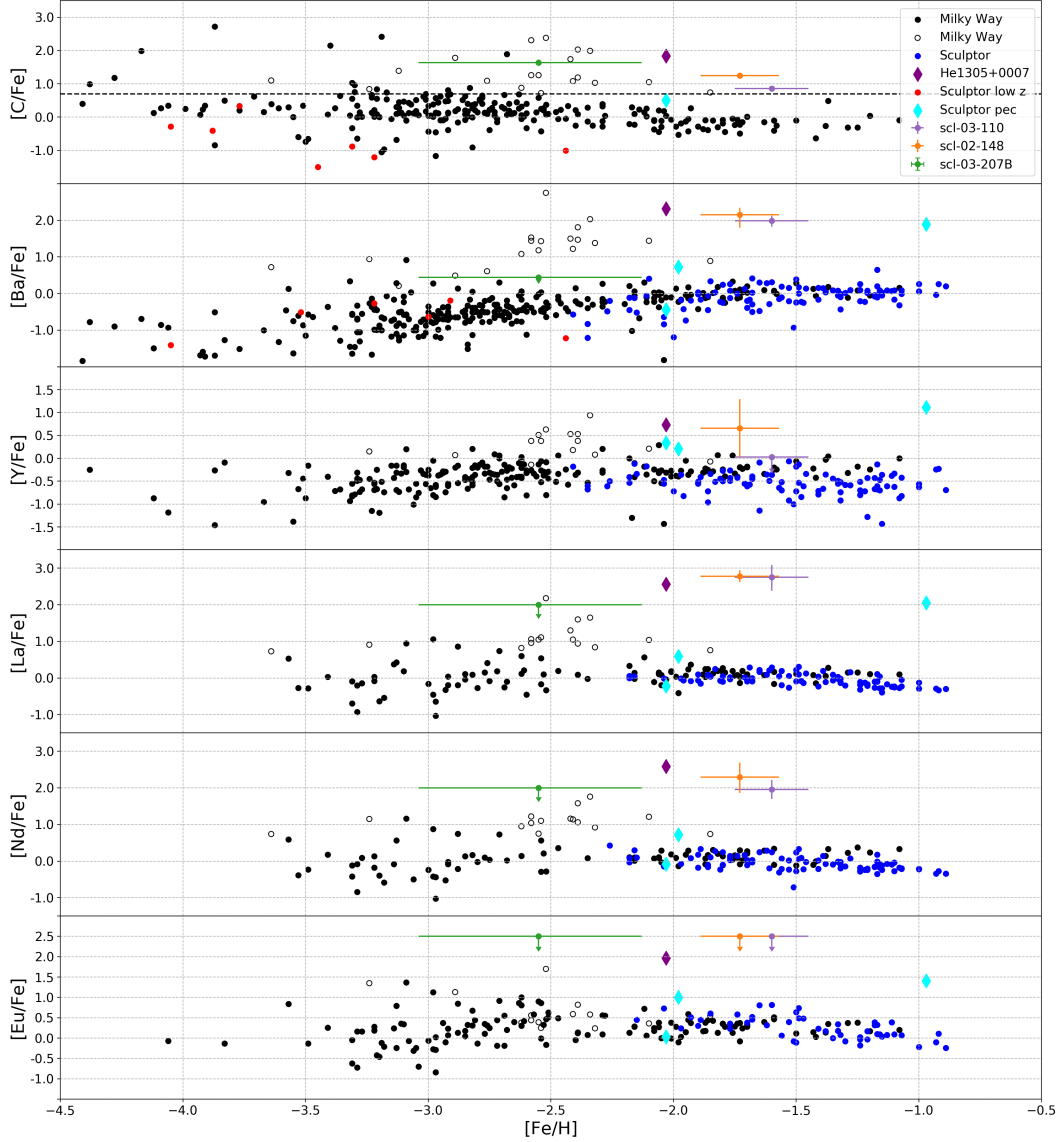
Figure 21: Abundance ratios of our stars compared with stars from the Milky Way and other Sculptor stars. Milky Way stars are given in black and are from Roederer et al. (2014) (open circles indicate CEMP stars with at least moderate s-process enhancement ([C/Fe] > 0.7 and [Ba/Fe] > 0.0). One more Milky Way star is shown as a purple diamond and is from Goswami et al. (2006). Sculptor stars in blue are from Hill et al. (2019) ([Fe/H]) and Skúladóttir et al. (2019) (other abundances). Low metallicity Sculptor stars in red are from Tafelmeyer et al. (2010), Starkenburg et al. (2013), Jablonka et al. (2015) and Simon et al. (2015). Three peculiar stars from Sculptor are shown as cyan diamonds. The star with [Fe/H] = -0.97 is from Geisler et al. (2005), the star with [Fe/H] = -1.98 is from Shetrone et al. (2003) and the star with [Fe/H] = -2.03 is from Skúladóttir et al. (2015). Finally our stars are shown in green, orange and purple. The dashed line at [C/Fe] = 0.7 indicates the threshold defined by Aoki et al. (2007) for CEMP stars.

Scl-03-207B shows more resemblance to the stars found by Shetrone et al. (2003) and Skúladóttir et al. (2015). Although it is more metal-poor and is more enriched in [C/Fe] compared to the other two stars in our sample, it only shows moderate [Ba/Fe] enhancement. Despite the fact that we can only give upper limits for [La/Fe] and [Nd/Fe] it is clear that this star is not as enhanced in these elements as scl-02-148 and scl-03-110 and may be similar to the 2 previously mentioned stars in these abundances.

Classifying scl-03-207B is slightly more challenging, it is clearly enhanced in [C/Fe] but it seems only moderately enhanced in [Ba/Fe]. Furthermore we can only determine upper limits for [La/Fe], [Nd/Fe] and [Eu/Fe]. CEMP stars with $0.0 < $ [Ba/Fe] $ < 1.0$ are not clearly defined by Beers & Christlieb (2005). We therefore classify this star as a CEMP star with moderate enhancement in s-process elements. One could speculate on how such a star could be formed. Does this star live in a binary system with a large orbit such that a small amount of mass transfer could have taken place? If one could determine whether this star lives in a binary system more can be said about the nature of the enhancement in this star. Measuring other s-process elements as well as the r-process element europium requires higher resolution measurements and will help classify this star in more detail.

Finally we can look into whether our stars have undergone mixing. If mixing has not taken place yet the atmosphere we observe consists of the same elemental abundances as the ISM in which the star has formed. This is why it is important to quantify whether our stars have been mixed. An example of this is that carbon is converted into nitrogen which is then dredged up to the surface. In this case we observe an overabundance of nitrogen and a underabundance of carbon compared to its original composition. In Spite et al. (2005) it is argued that metal-poor Milky Way halo stars with [C/N] > -0.4 are unmixed and stars with [C/N] < -0.4 are mixed. If we apply this definition to our stars it follows that scl-02-148 and scl-03-110 are not mixed with [C/N] = -0.16 and [C/N] = -0.31 respectively. However we expect CEMP-s stars to be more C than N rich so it is likely that some mixing has taken place. We do not know the original [C/N] ratio for these stars so we cannot say with complete confidence whether these stars have undergone mixing. Scl-03-207B is most likely not mixed with [C/N] = 0.86. This argument is strengthened by the fact that scl-03-207B has a higher T_{eff}, since warmer stars are more likely to be unmixed. One caveat is that most studies on mixing have been done on carbon normal stars. Lastly one needs to keep in mind that mixing is not an instant process and this happens gradually as stars move up the red giant branch.

If one properly wants to investigate whether stars have been mixed, there are stronger indicators than the [C/N] ratio. One example of this is the lithium abundance. Once mixing has taken place, the lithium abundance at the surface of the star decreases dramatically (Gratton et al., 2000). Another example is the $^{12}C/^{13}C$ ratio. This decreases as the amount of mixing increases. Unfortunately X-shooter observations do not allow us to measure either of these.

7 Conclusions

In this thesis we have successfully analysed X-shooter spectra of three CEMP stars in the Sculptor dwarf spheroidal. We have determined stellar parameters from photometry and created a line list with help of synthetic spectra. We have successfully normalized the continuum of our stars by using an iterative method making use of synthetic spectra. After normalization we have measured the abundances of carbon and nitrogen. For carbon this was done in the bandheads around 4400 Å, 4650 Å and 5100 Å. For nitrogen we used strong absorption in the CN region $6500 - 7500$Å.

The abundance of iron, as well as the abundances of neutron capture elements: barium, yttrium, lanthanum and neodymium were measured and upper limits were found for europium. We conclude that scl-02-148 and scl-03-110 show enhancement in s-process elements which these stars have likely obtained due to accretion from a binary companion. These stars are not likely to be r-process enhanced, therefore we classify scl-02-148 and scl-03-110 as CEMP-s stars. Scl-03-207B shows moderate enhancement in [Ba/Fe], and does not show an enhancement in r-process elements. This star cannot be classified using the classification scheme of Beers & Christlieb (2005). We conclude that this star is a CEMP star with a moderate enhancement in s-process elements and this star has likely not undergone internal mixing.

This thesis has shown that it is feasible to use X-shooter observations to determine abundances of CEMP stars in the Sculptor dwarf spheroidal. Abundances of carbon, nitrogen, iron, barium, lanthanum and neodymium can be determined accurately. Yttrium and europium likely require higher resolution spectroscopy to provide accurate measurements.

8 Acknowledgements

First and foremost I would like to thank prof. dr. Eline Tolstoy for giving me the opportunity to do a research project on CEMP stars and for her supervision during this time. We had fruitful discussions during our meetings, sometimes discussing other matters than astronomy as well. I would also like to thank her for asking me to help design the course "Stars, Nucleosynthesis and Chemical Evolution" as well as being the teaching assistant. I would also like to thank dr. Ása Skúladóttir for being the second supervisor to this project and being a tremendous help during the majority of the project. I am especially thankful for having spent two weeks in Heidelberg during which Ása taught me a lot about TURBOSPEC and measuring elemental abundances by use of synthetic spectra. On this note I would also like to thank the Kapteyn Institute for granting me the opportunity to visit the Max Planck Institute in Heidelberg.

Furthermore I would like to thank some of my fellow students who have probably heard me ramble too much about CEMP stars. I would like to thank Job for helping me whenever I had problems in Python and for helping me set up smart data structures. I would like to thank Sophie for our astronomy-related discussions and sanity checks during our research project. I would like to thank Lotte for keeping me sane during the final weeks of the project in which I had to work from home because of the outbreak of the Corona virus. Lastly I want to thank all other students in the master room who made sure there was a nice atmosphere.

Appendices

A Line List

Fe	4611.15	Y	4883.7
Fe	4733.7	Y	4900.1
Fe	4859.6	Y	5205.75
Fe	4920.4	La	5380.85
Fe	4957.5	La	5382.0
Fe	5005.7	La	5671.65
Fe	5168.9	La	5797.7
Fe	5195.2	La	6172.9
Fe	5226.8	La	6296.0
Fe	5232.8	La	6262.2
Fe	5250.4	La	6320.2
Fe	5269.75	La	6390.25
Fe	5283.7	La	6774.15
Fe	5328.2	Nd	4989.7
Fe	5371.5	Nd	5273.5
Fe	5397.15	Nd	5293.0
Ba	4934.1	Nd	5320.2
Ba	5853.65	Nd	5361.3
Ba	6141.9	Nd	5668.8
Ba	6496.9	Nd	5688.5
		Eu	6645.1

Table 4: The line list we use for abundance measurements. All values are given in Angstrom.

B Measurements

absorption line	scl-02-148	error_low	error_high	scl-03-110	error_low	error_high	scl-03-207B	error_low	error_high
Fe 4611.15	-1.8	0.58	0.0	-0.8	0.66	0.0	-1.96	0.99	0.0
Fe 4733.7	-2.29	0.0	0.52	-1.96	0.68	0.64	-2.67	0.0	0.52
Fe 4859.6	-1.97	0.7	0.91	-0.8	1.6	0.0	-2.78	0.57	0.0
Fe 4920.4	-1.51	0.0	0.56	-2.14	0.57	0.49	-1.98	0.58	0.44
Fe 4957.5	-1.87	0.35	0.32	-1.58	0.22	0.19	-2.77	0.17	0.17
Fe 5005.7	-1.44	0.48	0.5	-1.66	0.22	0.24	-2.87	0.55	0.5
Fe 5168.9	-2.08	0.63	0.69	-1.13	0.35	0.27	-3.5	0.0	0.17
Fe 5195.2	-0.9	0.52	0.0	-1.52	0.36	0.38	-3.5	0.0	0.6
Fe 5226.8	-1.53	0.32	0.3	-1.65	0.22	0.2	-3.13	0.0	0.35
Fe 5232.8	-1.17	0.36	0.3	-1.53	0.32	0.26	-3.5	0.0	0.28
Fe 5250.4	-1.21	0.46	0.0	-1.11	0.33	0.0	-3.5	0.0	0.76
Fe 5269.75	-1.79	0.44	0.35	-1.38	0.24	0.2	-3.14	0.0	0.34
Fe 5283.7	-1.02	0.28	0.0	-1.32	0.19	0.17	-2.61	0.67	0.56
Fe 5328.2	-1.97	0.37	0.33	-1.73	0.28	0.25	-3.5	0.0	0.4
Fe 5371.5	-1.64	0.0	0.0	-2.41	0.0	0.59	-3.02	0.0	1.46
Fe 5397.15	-2.5	0.0	0.64	-2.61	0.0	0.69	-3.5	0.0	0.48
Ba 4934.1	1.73	0.14	0.11	1.51	0.15	0.13	1.50	0.08	0.0
Ba 5853.65	2.17	0.49	0.0	2.13	0.23	0.18	0.26	0.0	0.13
Ba 6141.9	2.03	0.33	0.24	1.83	0.16	0.14	0.44	0.04	0.35
Ba 6496.9	2.27	0.16	0.13	2.01	0.1	0.09	0.44	0.03	0.11
Y 4883.7	0.66	0.63	0.63	-0.49	0.0	0.52	1.95	0.0	0.0
Y 4900.1	0.96	1.17	0.97	0.17	0.0	1.09	2.4	0.3	0.0
Y 5205.75	2.37	0.2	0.0	1.57	0.8	0.61	0.34	0.0	0.61
La 5380.85	4.0	0.49	0.0	3.51	0.67	0.0	2.5	0.27	0.0
La 5382.0	2.72	0.44	0.33	2.0	0.0	0.51	1.27	0.0	0.0
La 5671.65	2.7	0.0	0.63	2.0	0.0	0.56	1.27	0.0	0.0
La 5797.7	2.6	0.0	0.66	2.32	0.0	0.73	1.26	0.0	0.14
La 6172.9	2.69	0.59	0.58	2.0	0.0	0.2	2.5	0.0	0.0
La 6296.0	2.62	0.35	0.36	2.0	0.0	0.32	2.5	0.42	0.0
La 6262.2	3.09	0.22	0.21	2.0	0.0	0.81	1.44	0.89	0.26
La 6320.2	2.52	0.37	0.35	2.36	0.29	0.29	1.45	0.06	0.24
La 6390.25	2.68	0.35	0.34	2.92	0.36	0.34	0.5	0.0	1.28
La 6774.15	3.12	0.42	0.36	2.98	0.46	0.4	1.8	0.16	0.13
Nd 4989.7	2.48	0.32	0.36	2.18	0.18	0.2	2.5	0.24	0.0
Nd 5273.5	3.0	0.77	0.0	2.68	0.77	0.0	1.8	0.79	0.0
Nd 5293.0	3.0	0.25	0.0	2.9	0.59	0.0	2.4	0.56	0.0
Nd 5320.2	2.1	0.72	0.58	1.01	0.0	0.8	1.26	0.0	0.73
Nd 5361.3	2.29	0.26	0.26	1.67	0.19	0.18	1.99	0.34	0.3
Nd 5668.8	3.0	0.19	0.0	2.41	0.28	0.29	0.87	0.0	1.31
Nd 5688.5	2.53	0.57	0.0	1.62	0.37	0.38	0.87	0.0	0.34
Eu 6645.1	1.64	1.06	0.43	1.47	0.97	0.43	0.68	0.0	0.63

Table 5: All individual line measurements for all stars.

References

Alvarez, R., & Plez, B. 1998, A&A, 330, 1109. https://arxiv.org/abs/astro-ph/9710157

Aoki, W., Beers, T. C., Christlieb, N., et al. 2007, ApJ, 655, 492, doi: 10.1086/509817

Azzopardi, M., Lequeux, J., & Westerlund, B. E. 1985, A&A, 144, 388

Battaglia, G., Irwin, M., Tolstoy, E., et al. 2008, MNRAS, 383, 183, doi: 10.1111/j.1365-2966.2007.12532.x

Beer, H., Walter, G., Macklin, R. L., & Patchett, P. J. 1984, , 30, 464, doi: 10.1103/PhysRevC.30.464

Beers, T. C., & Christlieb, N. 2005, ARA&A, 43, 531, doi: 10.1146/annurev.astro.42.053102.134057

Bisterzo, S., Gallino, R., Straniero, O., Cristallo, S., & Käppeler, F. 2011, MNRAS, 418, 284, doi: 10.1111/j.1365-2966.2011.19484.x

Blackwell, D. E., & Shallis, M. J. 1977, MNRAS, 180, 177, doi: 10.1093/mnras/180.2.177

Burbidge, E. M., Burbidge, G. R., Fowler, W. A., & Hoyle, F. 1957, Reviews of Modern Physics, 29, 547, doi: 10.1103/RevModPhys.29.547

Chiti, A., Simon, J. D., Frebel, A., et al. 2018, ApJ, 856, 142, doi: 10.3847/1538-4357/aab663

Cowan, J. J., & Rose, W. K. 1977, ApJ, 212, 149, doi: 10.1086/155030

Dardelet, L., Ritter, C., Prado, P., et al. 2015, arXiv e-prints, arXiv:1505.05500. https://arxiv.org/abs/1505.05500

de Boer, T. J. L., Tolstoy, E., Hill, V., et al. 2012, A&A, 539, A103, doi: 10.1051/0004-6361/201118378

Gallagher, A. J., Ryan, S. G., García Pérez, A. E., & Aoki, W. 2010, A&A, 523, A24, doi: 10.1051/0004-6361/201014970

Geisler, D., Smith, V. V., Wallerstein, G., Gonzalez, G., & Charbonnel, C. 2005, AJ, 129, 1428, doi: 10.1086/427540

Gonneau, A., Lyubenova, M., Lançon, A., et al. 2020, arXiv e-prints, arXiv:2001.03080. https://arxiv.org/abs/2001.03080

Goswami, A., Aoki, W., Beers, T. C., et al. 2006, MNRAS, 372, 343, doi: 10.1111/j.1365-2966.2006.10877.x

Gratton, R. G., Sneden, C., Carretta, E., & Bragaglia, A. 2000, A&A, 354, 169

Grevesse, N., & Sauval, A. J. 1998, , 85, 161, doi: 10.1023/A:1005161325181

Gustafsson, B., Edvardsson, B., Eriksson, K., et al. 2008, A&A, 486, 951, doi: 10.1051/0004-6361:200809724

Hampel, M., Stancliffe, R. J., Lugaro, M., & Meyer, B. S. 2016, ApJ, 831, 171, doi: 10.3847/0004-637X/831/2/171

Hansen, C. J., Nordström, B., Hansen, T. T., et al. 2016, A&A, 588, A37, doi: 10.1051/0004-6361/201526895

Hartwig, T., & Yoshida, N. 2019, ApJ, 870, L3, doi: 10.3847/2041-8213/aaf866

Hill, V., Skúladóttir, Á., Tolstoy, E., et al. 2019, A&A, 626, A15, doi: 10.1051/0004-6361/201833950

Hinkle, K., Wallace, L., Valenti, J., & Harmer, D. 2000, Visible and Near Infrared Atlas of the Arcturus Spectrum 3727-9300 A

Ishigaki, M. N., Tominaga, N., Kobayashi, C., & Nomoto, K. 2014, ApJ, 792, L32, doi: 10.1088/2041-8205/792/2/L32

Jablonka, P., North, P., Mashonkina, L., et al. 2015, A&A, 583, A67, doi: 10.1051/0004-6361/201525661

Kirby, E. N., Guhathakurta, P., Bolte, M., Sneden, C., & Geha, M. C. 2009, ApJ, 705, 328, doi: 10.1088/0004-637X/705/1/328

Kirby, E. N., Guo, M., Zhang, A. J., et al. 2015, ApJ, 801, 125, doi: 10.1088/0004-637X/801/2/125

Kupka, F., Piskunov, N., Ryabchikova, T. A., Stempels, H. C., & Weiss, W. W. 1999, , 138, 119, doi: 10.1051/aas:1999267

Lee, Y. S., Beers, T. C., Masseron, T., et al. 2013, AJ, 146, 132, doi: 10.1088/0004-6256/146/5/132

Maeder, A., & Meynet, G. 2015, A&A, 580, A32, doi: 10.1051/0004-6361/201526234

Matrozis, E., Ryde, N., & Dupree, A. K. 2013, A&A, 559, A115, doi: 10.1051/0004-6361/201322317

Pietrzyński, G., Gieren, W., Szewczyk, O., et al. 2008, AJ, 135, 1993, doi: 10.1088/0004-6256/135/6/1993

Pignatari, M., Gallino, R., Heil, M., et al. 2010, ApJ, 710, 1557, doi: 10.1088/0004-637X/710/2/1557

Placco, V. M., Frebel, A., Beers, T. C., & Stancliffe, R. J. 2014, ApJ, 797, 21, doi: 10.1088/0004-637X/797/1/21

Plez, B. 2012, Turbospectrum: Code for spectral synthesis, Astrophysics Source Code Library. http://ascl.net/1205.004

Ramírez, I., & Meléndez, J. 2005, ApJ, 626, 465, doi: 10.1086/430102

Ratzel, U., Arlandini, C., Käppeler, F., et al. 2004, , 70, 065803, doi: 10.1103/PhysRevC. 70.065803

Roederer, I. U., Karakas, A. I., Pignatari, M., & Herwig, F. 2016, ApJ, 821, 37, doi: 10. 3847/0004-637X/821/1/37

Roederer, I. U., Preston, G. W., Thompson, I. B., et al. 2014, AJ, 147, 136, doi: 10. 1088/0004-6256/147/6/136

Rudolf, N., Günther, H. M., Schneider, P. C., & Schmitt, J. H. M. M. 2016, A&A, 585, A113, doi: 10.1051/0004-6361/201322749

Shetrone, M., Venn, K. A., Tolstoy, E., et al. 2003, AJ, 125, 684, doi: 10.1086/345966

Shetrone, M. D., Briley, M., & Brewer, J. P. 1998, A&A, 335, 919

Simon, J. D., Jacobson, H. R., Frebel, A., et al. 2015, ApJ, 802, 93, doi: 10.1088/ 0004-637X/802/2/93

Skúladóttir, Á., Hansen, C. J., Choplin, A., et al. 2020, A&A, 634, A84, doi: 10.1051/ 0004-6361/201937075

Skúladóttir, Á., Hansen, C. J., Salvadori, S., & Choplin, A. 2019, A&A, 631, A171, doi: 10.1051/0004-6361/201936125

Skúladóttir, Á., Tolstoy, E., Salvadori, S., et al. 2015, A&A, 574, A129, doi: 10.1051/ 0004-6361/201424782

Sneden, C., Cowan, J. J., & Gallino, R. 2008, ARA&A, 46, 241, doi: 10.1146/annurev. astro.46.060407.145207

Spite, M., Cayrel, R., Plez, B., et al. 2005, A&A, 430, 655, doi: 10.1051/0004-6361: 20041274

Starkenburg, E., Hill, V., Tolstoy, E., et al. 2013, A&A, 549, A88, doi: 10.1051/ 0004-6361/201220349

Starkenburg, E., Shetrone, M. D., McConnachie, A. W., & Venn, K. A. 2014, MNRAS, 441, 1217, doi: 10.1093/mnras/stu623

Starkenburg, E., Hill, V., Tolstoy, E., et al. 2010, A&A, 513, A34, doi: 10.1051/ 0004-6361/200913759

Tafelmeyer, M., Jablonka, P., Hill, V., et al. 2010, A&A, 524, A58, doi: 10.1051/ 0004-6361/201014733

Tolstoy, E., Irwin, M. J., Helmi, A., et al. 2004, ApJ, 617, L119, doi: 10.1086/427388

Vernet, J., Dekker, H., D'Odorico, S., et al. 2011, A&A, 536, A105, doi: 10.1051/0004-6361/201117752

Watson, D., Hansen, C. J., Selsing, J., et al. 2019, Nature, 574, 497, doi: 10.1038/s41586-019-1676-3